UNIVERSITÀ DEGLI STUDI DI PADOVA

DIPARTIMENTO DI BIOLOGIA

Corso di Laurea in Biologia Molecolare

ELABORATO DI LAUREA

REGOLAZIONE DELLA SINTESI DI dNTPs IN SEGUITO A DANNO AL DNA IN CELLULE DI MAMMIFERO

Tutor: Prof.ssa Chiara Rampazzo
Dipartimento di Biologia

Laureando: Giacomo Birro

ANNO ACCADEMICO 2022/2023

Abbreviazioni

Composti

ADP = Adenosina difosfato

AMP = Adenosina monofosfato

BrdU = Bromodeossiuridina

dATP = Deossiadenosina trifosfato

dNTP = Deossiribonucleotide

GFP = *Green Fluorescent Protein*

GMP = Guanosina monofosfato

IMP = Inosina monofosfato

PRPP = Fosforibosilpirofosfato

R5P = Ribosio 5-fosfato

sgRNA = *Single-guide RNA*

shRNA = *Short Hairpin RNA*

siRNA = *Small Interfering RNA*

Enzimi

ATM = *Ataxia-Telangiectasia Mutated*

cGAS = *Cyclic GMP-AMP synthase*

PRPS = Fosforibosilpirofosfato Sintasi

RNR = Ribonucleotide Reduttasi

SAMHD1 = *SAM domain and HD domain-containing protein 1*

STING = *Stimulator of interferon genes*

TBK1 = *TANK-binding kinase 1*

TREX1 = *Three prime repair exonuclease 1*

Altre abbreviazioni

DSB = *Double Strand Break*

HPLC = *High Performance Liquid Chromatography*

HR = *Homologous Recombination*

HRMS = *High Resolution Mass Spectrometry*

IR = *Ionizing Radiation*

NHEJ = *Non-Homologous End Joining*

PCR = *Polymerase Chain Reaction*

PPP = *pentose phosphate pathway*

WT = *Wild Type*

Indice

Capitolo 0 – Abstract

I danni al DNA da radiazione ionizzante (IR) causano instabilità genomica e sono altamente citotossici. Il metabolismo dei deossiribonucleotidi (dNTPs) provvede a garantire gli elementi necessari alla riparazione del DNA.
L'articolo analizzato in questo elaborato suggerisce come il trattamento con radiazioni ionizzanti in cellule di mammifero porti alla fosforilazione dell'enzima fosforibosilpirofosfato sintetasi (PRPS1/2) in posizione T228 mediata da TBK1. La fosforilazione di PRPS1/2 ne aumenterebbe l'attività catalitica, portando ad un incremento della concentrazione di PRPP (molecola necessaria nel metabolismo dei dNTPs). L'articolo analizza anche come tale fosforilazione necessiti però dell'attivazione del sistema immunitario innato mediante il *pathway* cGAS/STING e di una precedente fosforilazione di PRPS1/2 in posizione S16 da parte della chinasi ATM.
Gli autori suggeriscono che l'attivazione di PRPS1/2 porti anche ad un aumento del *pool* di dNTPs. Ciò appare tuttavia in contrasto con quanto riportato in letteratura in relazione a cellule di mammifero, dove le concentrazioni di dNTPs non tendono ad aumentare dopo danno al DNA da radiazioni ionizzanti. L'enzima della tappa *rate-limiting* nella sintesi di dNTPs, ossia la RNR, è regolato allostericamente ed è in grado di controllare le concentrazioni dei precursori del DNA.
Questo elaborato si pone dunque a discutere i risultati sperimentali ottenuti dagli autori tramite un confronto con la relativa letteratura.

Capitolo 1 – Stato dell'arte

Un fattore cruciale per mantenere la stabilità del genoma è la disponibilità dei deossiribonucleotidi trifosfato (dNTPs) all'interno di un intervallo ottimale per la replicazione e riparazione del DNA.

In lievito il danno al DNA è associato ad un aumento del *pool* di dNTPs grazie all'inibizione allosterica "rilassata" della ribonucleotide reduttasi (RNR), mentre questo non avviene in cellule di mammifero. In letteratura infatti è stato più volte dimostrato che nei mammiferi mancano i meccanismi molecolari coinvolti nell'attivazione della RNR in seguito a danni al DNA.

Gli autori dell'articolo analizzato non solo osservano un aumento del pool dei dNTPs dopo danni al DNA ma propongono anche un *pathway* alternativo per la regolazione della sintesi di dNTPs in cellule di mammifero.

1.1 Panoramica sui livelli di dNTPs durante la fase S in eucarioti

[1] Nel contesto della replicazione del DNA, l'attivazione di enzimi implicati nello svolgimento della doppia elica e nella sintesi del DNA deve essere coordinata con l'aumento della disponibilità di dNTPs. Infatti, il *pool* di dNTPs durante la fase S è solo sufficiente a replicare una piccola frazione del genoma ed è l'aumentata espressione di alcuni enzimi a garantire la sintesi del DNA. Il processo replicativo in fase S è associato ad un aumento di attività dell'enzima ribonucleotide reduttasi (RNR), enzima chiave nella sintesi *de novo* dei dNTPs. Questo enzima viene regolato tramite diversi meccanismi: attivazione allosterica, aumentati livelli di espressione della subunità R2 e proteolisi delle proteine che inibiscono l'enzima. Contribuiscono al rifornimento di dNTPs anche due *pathway* di recupero, uno citosolico e uno mitocondriale, dove deossiribonucleosidi ottenuti dalla degradazione del DNA o importati dall'ambiente extracellulare vengono fosforilati fino alle forme trifosfato.

La concentrazione dei dNTPs dipende non solo dalle vie sintetiche ma anche dalle vie degradative, dove SAMHD1, una dNTP trifosfoidrolasi, è l'enzima principale. Questo enzima degrada i dNTPs a deossinucleosidi e trifosfato e contribuisce assieme alla RNR a garantire una concentrazione bilanciata dei 4 precursori del DNA durante le diverse fasi del ciclo cellulare.

1.2 Ribonucleotide reduttasi (RNR)

[2] In tutti gli organismi, l'enzima ribonucleotide reduttasi sintetizza i quattro deossiribonucleotidi trifosfato (dNTPs), richiesti per la replicazione e riparazione del DNA, attraverso la sostituzione del gruppo 2'-OH di un ribonucleoside di- o tri-fosfato con un atomo di idrogeno. Una caratteristica comune di tutte queste reduttasi è la loro abilità di provvedere ad un appropriato equilibrio tra le quattro tipologie di deossinucleotidi del DNA e ciò che rende questo possibile è una particolare regolazione allosterica della loro specificità di substrato. Le RNRs possono essere raggruppate in tre differenti classi (I, II, III) sulla base della loro interazione con l'ossigeno e per la modalità di generazione del radicale tiile necessario al processo

catalitico. Tutti gli eucarioti, da lievito a uomo, possiedono RNR di classe I, in particolare Ia.

Le RNR di classe I infatti comprendono i due sottogruppi Ia e Ib, aventi strutture primarie leggermente diverse. Entrambi i sottogruppi contengono due subunità dimeriche diverse (R1 e R2) che compongono complessivamente un tetramero eterodimerico. La subunità maggiore R1 è un omodimero e contiene il sito catalitico, un sito redox disulfidico coinvolto nella riduzione dei ribonucleotidi e due siti allosterici. La subunità minore R2 è anch'essa un omodimero e contiene un radicale tirosilico indispensabile per la riduzione radicalica del substrato.

1.3 Regolazione della sintesi di dNTPs in mammifero dopo danno al DNA

[3] [4] A differenza degli eucarioti unicellulari come lievito, dove il danno al DNA porta a un incremento nell'attività di RNR e ad un aumento del *pool* di dNTPs, le cellule di mammifero non mostrano alcun aumento significativo nelle dimensioni del *pool* di dNTPs in risposta a danno al DNA.

Come descritto nel paragrafo precedente, le cellule di mammifero contengono due subunità non identiche di RNR. Si tratta di una subunità grande omodimerica R1 (contenente il sito catalitico) e di una tra due varianti della subunità piccola omodimerica, ossia R2 o p53R2, ciascuna contente il radicale libero tirosile essenziale per la catalisi. La replicazione del DNA in fase S è supportata da una RNR composta dalle subunità R1 ed R2, mentre, in seguito a danno al DNA viene indotta l'espressione della subunità p53R2.

Tuttavia, né cellule di mammifero in crescita logaritmica, né in fase G_0/G_1, mostrano incrementi significativi nei propri *pools* di dNTPs dopo danno al DNA. Il lento aumento di 4 volte nell'espressione di p53R2 dopo danno al DNA risulta in un aumento di meno di 2 volte nel *pool* di dNTPs in cellule G_0/G_1, che invece viene ad essere solo il 5% di quello presente in fase S.

È fondamentale notare che l'attività delle RNRs eucariotiche subisce un'inibizione allosterica da dATP, anche se il grado di inibizione differisce tra le RNRs delle diverse specie. In lievito la RNR non è inibita da dATP nel range tra 0 e 20 μM, mentre presenta un'inibizione solo del 20% della sua attività con dATP 50 μM. Si osserva quindi un'inibizione da dATP "rilassata", che permette un innalzamento nel *pool* di dNTPs fino a 8 volte in seguito a danno al DNA.

Al contrario, l'attività della RNR in uomo è fortemente inibita anche a basse concentrazioni di dATP: RNR di uomo purificata perde circa il 30% della propria attività in presenza di dATP 2.5 μM; mentre arriva a perdere il 50% dell'attività in presenza di dATP 5 μM. È interessante notare che l'inattivazione in eterozigosi del sito allosterico nella subunità R1 mediante la sostituzione di un aspartato in posizione 57 con asparagina è sufficiente a far aumentare il *pool* di dNTPs fino a 9 volte.

1.4 Effetti cellulari di alti livelli di dNTPs

L'assenza di un incremento nel *pool* di dNTPs in cellule di mammifero dopo danno al DNA trova significato dal punto di vista evolutivo. L'espansione del *pool* di dNTPs può infatti avere conseguenze sulla fedeltà nella replicazione ed essere correlato ad un aumento del tasso di mutazione.

In mammifero è possibile indurre alti livelli di dNTPs tramite l'inattivazione dell'inibizione a feedback da dATP di RNR, oppure tramite la sovra-espressione delle subunità di RNR, o inattivando SAMHD1.

Elevate concentrazioni di dNTPs risultano diminuire la fedeltà della replicazione del DNA sia in batteri, sia in lievito e cellule di mammifero. Infatti, alte concentrazioni di dNTPs sono state riconosciute da molto tempo come un fattore che riduce la capacità *proofreading* di enzimi DNA polimerasi.

In vivo, l'abilità della polimerasi a bassa fedeltà per sintesi translesione (TLS) di subentrare alle normali polimerasi replicative potrebbe essere aumentata da alti livelli di dNTPs. Infatti, TLS possiede una più alta costante di affinità (K_m) per dNTPs rispetto a Pol δ e Pol ε, ossia le DNA polimerasi responsabili rispettivamente della sintesi dei filamenti *lagging* e *leading* in eucarioti. Come previsto, l'inattivazione delle polimerasi TLS porta ad una riduzione dei tassi di mutazione associati ad elevati livelli di dNTPs.

1.5 Una nuova via di regolazione per la sintesi di dNTPs in seguito a danno al DNA

L'obiettivo degli autori è stato quello di studiare le conseguenze dell'interazione tra due enzimi con attività di chinasi, ossia ATM e TBK1, e un terzo enzima, PRPS1/2, il quale è implicato nella sintesi di PRPP (molecola essenziale nella sintesi dei dNTPs), in un contesto di danno al DNA dato da radiazioni ionizzanti.

Gli autori hanno condotto i loro esperimenti in tre diverse linee cellulari (cellule epiteliali intestinali umane FHs74, cheratinociti orali umani HOKs e cellule endoteliali del cordone ombelicale umane HUVECs) e hanno introdotto rotture a doppio filamento (DSB) trattandole con radiazioni ionizzanti. Il trattamento causa l'attivazione della chinasi ATM, che fosforila PRPS1/2 in posizione S16. In un momento successivo, l'attivazione del *pathway* cGAS-STING-TBK1 porta alla fosforilazione sempre di PRPS1/2 in T228.

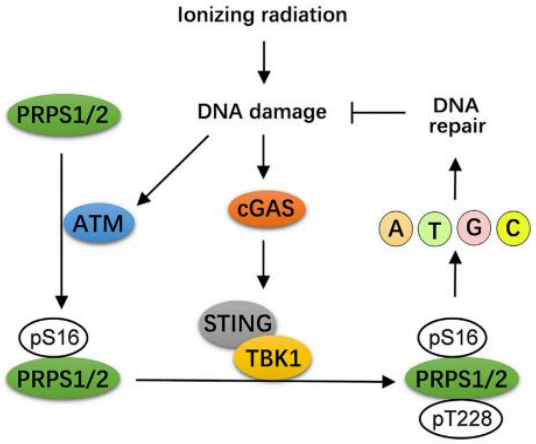

Figura 1. Riassunto dei pathways esaminati dallo studio. [10]

Esperimenti ulteriori condotti dagli autori mostrano che le fosforilazioni in diversi siti di PRPS1/2 inibiscono la regolazione allosterica data da precursori dei dNTPs (come ADP, IMP, GMP, AMP) che PRPS1/2 normalmente subisce, favorendo un aumento della sintesi di PRPP e del *pool* di dNTPs necessari alla riparazione dei DSBs.

[5] ATM è una serina/treonina chinasi principalmente nota per orchestrare processi di riparazione del DNA in seguito a rotture a doppio filamento (DSBs). Mutazioni nel gene ATM portano ad Atassia-Teleangectasia (AT o Sindrome di Louis-Bar). In seguito al reclutamento ed all'attivazione da DSBs, ATM fosforila diverse proteine chiave, soprattutto soppressori tumorali, che portano all'attivazione del checkpoint da danno al DNA, all'arresto del ciclo cellulare, alla riparazione del DNA o apoptosi.

[6] Il *pathway* cGAS-STING-TBK1 invece è ad oggi apprezzato come la principale via di segnalazione nella risposta immunitaria innata in uomo. La via combina il rilevamento di DNA citosolico con l'induzione di un forte programma innato di difesa immunitaria, comprendente l'attivazione di geni legati a infiammazione che possono portare a senescenza o all'attivazione di altri meccanismi di difesa. Attraverso il riconoscimento di DNA esogeno di virus e batteri oppure di DNA endogeno danneggiato, cGAS (presentante un *DNA binding site*) catalizza poi la sintesi di cGAMP da ATP e GTP. cGAMP interagisce poi con STING e il complesso attiva *pathways* a valle inducendo l'espressione di interferoni di tipo I e citochine pro-infiammatorie. Il complesso STING-cGAMP può reclutare poi TBK1, chinasi tra le cui funzioni c'è l'attivazione di IRF3 (Interferon regulatory factor 3).

PRPS è invece un enzima che converte ribosio-5-fosfato in fosforibosil pirofosfato (PRPP). PRPP è utilizzato poi in *pathways* di biosintesi dei nucleotidi, in quanto PRPP provvede a donare il proprio zucchero ribosio nella sintesi *de novo* di purine e pirimidine (vedi *figura 2*). Tre sono le PRPS identificate in uomo, codificate da 3 geni diversi ma con sequenza molto simile. PRPS1 e PRPS2 sono espresse nella maggior parte degli organi (PRPS3 solo in testicolo). PRPS1/2 è regolata tramite fosforilazione e allosteria. Viene attivata da fosfato e inibita da ADP: si suggerisce che fosfato e ADP competano per lo stesso sito regolatorio. È importante sottolineare che ADP viene considerato l'inibitore allosterico chiave dell'enzima.

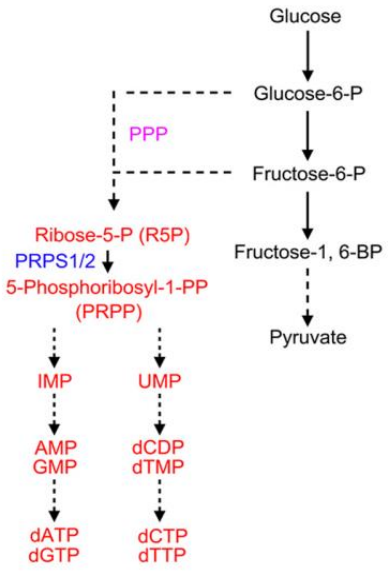

Figura 2. Pathway glicolitico di sintesi dei dNTPs. [10]

Capitolo 2 – Approccio sperimentale e metodologie

2.1 Impiego di linee cellulari

Le linee cellulari impiegate nello studio sono tutte linee cellulari primarie umane. FHs 74 Int sono cellule epiteliali dell'intestino tenue; HUVECs sono cellule endoteliali della vena ombelicale; HOKs sono cheratinociti orali. Tutte queste linee sono note per rispondere all'esposizione con radiazioni ionizzanti attivando meccanismi di riparazione del danno al DNA. L'importanza dell'utilizzo di linee primarie risiede nel fatto che cellule tumorali mostrano un alterato metabolismo dei dNTPs, necessario a supportare divisioni rapide e incontrollate; si tratterebbe quindi di un modello inadatto a studi riguardanti il metabolismo di dNTPs in condizioni fisiologiche.

2.2 Sincronizzazione del ciclo cellulare con lovastatina e analisi del ciclo cellulare tramite citofluorimetria

[7] Un protocollo di sincronizzazione cellulare consente di ottenere una frazione di cellule in una specifica fase del ciclo cellulare partendo da una popolazione asincrona. Le tecniche di sincronizzazione prevedono un approccio di tipo chimico o fisico: per sincronizzare le cellule in fase G1 è stata scelta una metodica chimica basata sull'impiego di lovastatina. La lovastatina è un inibitore dell'enzima HMG-CoA reduttasi, implicato nella sintesi di mevalonato. Il meccanismo di azione della lovastatina sembra però riguardare indirettamente l'inibizione del proteasoma, alla quale consegue un accumulo di p21, inibitore della chinasi CDK2 necessaria per la transizione G1/S. Per valutare la sincronizzazione cellulare è stata studiata la distribuzione delle cellule nelle diverse fasi del ciclo cellulare tramite western blot, valutando l'espressione di diverse cicline. La ciclina E, ad esempio, viene espressa in tarda fase G1, la ciclina A durante la fase S mentre la ciclina B durante le fasi G2/M. Le cellule sono state lavate due volte con PBS prima del trattamento con lovastatina 20 μM per 24 ore. Successivamente sono state incubate nuovamente in terreno fresco.

Per l'analisi del ciclo cellulare tramite citofluorimetria, le cellule sono state fissate con etanolo al 70% in ghiaccio per 30 minuti, lavate con PBS e risospese in 100 μg/ml RNasi A in PBS per altri 30 minuti. Dopo l'incubazione, le cellule sono state colorate con ioduro di propidio, intercalante fluorescente che lega stechiometricamente il DNA ed è eccitabile a 488 nm emettendo a 625 nm. Il trattamento con RNasi A è necessario in quanto lo ioduro di propidio è in grado di legare anche molecole di RNA: ciò potrebbe compromettere l'analisi di citofluorimetria, che invece si basa solo sullo *staining* di DNA. È stata quindi poi effettuata un'analisi di citofluorimetria a flusso. In questa procedura le cellule sono sospese in un fluido e iniettate nel citofluorimetro; le singole cellule sono incanalate in un foro molto stretto, in modo da creare un flusso all'interno del quale esse sono organizzate in una fila. Le cellule passano poi attraverso un laser che le colpisce una ad una. Lo scattering della luce, ossia le modalità con cui questa viene

distribuita nella stessa direzione del fascio di luce (*forward scatter*), o lateralmente (*side scatter*), fornisce informazioni rispettivamente sulle dimensioni e sulla complessità interna della cellula. Lo scattering della luce è misurato da un detector. In questo caso, la variabile analizzata è l'intensità della fluorescenza emessa dallo ioduro di propidio, presente nel *side scatter* e funzione della quantità di DNA nella singola cellula. Cellule in fase S avranno più DNA rispetto a cellule in fase G1, e cellule in fase G2/M emetteranno una fluorescenza di intensità doppia rispetto alle cellule in fase G1. Il software *FlowJo 10.4* ha poi permesso di calcolare le percentuali di cellule in fase G1, S e G2/M.

2.3 Irraggiamento delle cellule

La radiazione ionizzante è stata ottenuta tramite un irraggiatore Cr^{137} γ-ray a 2 Gy/min a temperatura ambiente. Dopo aver rimosso il mezzo di coltura le cellule vengono irradiate. Mezzo di coltura fresco viene aggiunto subito dopo.

2.4 *RNA interference* tramite shRNAs

L'RNA interference (RNAi) è un meccanismo che consente l'inibizione dell'espressione genica a livello post trascrizionale. La traduzione di un messaggero può essere cioè inibita tramite un siRNA (*small interfering RNA*) avente una sequenza reverso-complementare ad un tratto della sequenza del trascritto. Per ottenere un silenziamento transiente è possibile iniettare direttamente il siRNA; per un silenziamento non-transiente è possibile trasfettare le cellule con plasmidi che consentano la trascrizione di un precursore del siRNA, detto shRNA (*short hairpin RNA*). Lo shRNA viene poi processato in siRNA dall'enzima Dicer. Qui, gli autori hanno utilizzato tale metodologia per ottenere il silenziamento genico di cGAS, STING, TBK1 e PRPS1/2. Il vettore per la trascrizione del shRNA è stato quindi *trasfettato* nelle cellule. Il plasmide contiene anche la sequenza codificante per la resistenza all'antibiotico puromicina, che consente di selezionare le cellule che hanno integrato in modo stabile nel genoma il vettore.

2.5 Studio dell'interazione di PRPS1/2 con ADP

Per dimostrare come la fosforilazione in T228 diminuisca l'interazione tra PRPS1/2 e ADP, sono state prese in considerazione PRSP1 e PRPS2, sia in versione *wild type* che in versione mutante non fosforilabile in T228. Secondo gli autori infatti, dopo la fosforilazione da parte di ATM e TBK1, l'enzima PRPS1/2 subisce una riduzione dell'inibizione allosterica da parte di intermedi dei nucleotidi (come ADP, AMP, IMP e GMP). Le proteine PRPS sono state allora sottoposte ad una fosforilazione in vitro da parte di ATM e successivamente di TBK1, per indurre la fosforilazione in T228 nelle proteine *wild type*. In seguito, gli enzimi PRPS sono stati incubati con [^{14}C]-ADP, ossia ADP radioattiva, per 12 ore, in un buffer di binding (Tris-HCl 50 mM, pH 7.5, KCl 100 mM, $MgCl_2$ 50 mM, Na_3VO_4 1 mM, DTT 1 mM, 5% glicerolo). Le proteine sono state poi lavate e infine la radioattività è stata misurata tramite uno scintillatore e utilizzata come misura indiretta della tendenza di PRPS1/2 ad interagire con ADP. Una maggiore radioattività corrisponde ad una maggiore interazione tra PRPS1/2 e ADP.

2.6 Misurazione dell'attività enzimatica di PRPS1/2

Per dimostrare come, dopo il trattamento delle cellule con IR, mutanti di PRPS1/2 non fosforilabili in T228 abbiano minore attività rispetto agli enzimi *wild type*, è stato necessario effettuare un saggio di misurazione dell'attività enzimatica tramite analisi spettrofotometrica. Il valore di assorbanza del sistema è stato misurato a 340 nm (ossia il picco di assorbimento di NADH) in modalità cinetica per 5 minuti, mentre veniva eseguito il sistema di reazioni descritto in seguito:

a. PRPS1/2 catalizza: ATP + R5P → PRPP + AMP;
b. Miochinasi catalizza: ATP + AMP → ADP;
c. Piruvato chinasi catalizza: fosfoenolpiruvato + ADP → piruvato + ATP;
d. Lattato deidrogenasi catalizza: piruvato + NADH → lattato + NAD.

La riduzione del segnale di assorbanza a 340 nm, il picco di assorbimento di NADH, indica la disponibilità di piruvato, che riflette la produzione di ADP e dunque l'attività catalitica di PRPS1/2. Tanto più velocemente si riduce il segnale di assorbanza a 340 nm, tanto maggiore è l'attività di PRPS1/2.
Proteine PRPS1 e PRPS2 batteriche purificate mediante His-tag sono state sequenzialmente trattate con ATM e TBK1 per indurre la fosforilazione di PRPS1/2 in T228. Successivamente, 10 ng di proteine PRPS sono stati incubati in 100 µl di buffer di reazione (50 mmol/l Tris-HCl [pH 7.5], 0.4 mmol/l NADH, 1.8 mmol/l fosfoenolpiruvato, 6 mmol/l $MgCl_2$, 31 mmol/l $NaHCO_3$, 7 U piruvato chinasi, 10 U lattato deidrogenasi, 10 U miochinasi). Miochinasi, piruvato chinasi, lattato deidrogenasi e fosfoenolpiruvato sono state inserite in eccesso nel sistema per permettere il completo consumo dell'AMP prodotto da PRPS1/2.

2.7 Produzione di mutanti PRPS1/2 tramite CRISPR-Cas9

Per verificare la specificità della fosforilazione nel residuo T228 di PRPS1/2, è stata effettuata mutagenesi sito-specifica su cellule FHs 74 Int con l'obiettivo di isolare mutanti presentanti PRPS1/2 non fosforilabile in tale posizione. La scelta della strategia di *editing* genomico è ricaduta sul sistema CRISPR-Cas9. Il sistema CRISPR-Cas9 si basa sull'introduzione in una cellula bersaglio dei geni che codificano per la proteina con attività nucleasica Cas9 e per un sgRNA (*single-guide RNA*). Il sgRNA avrà una regione complementare alla sequenza del genoma da modificare. Nella cellula si forma un complesso dato dal sgRNA e dalla proteina Cas9, che arriverà quindi in prossimità del sito bersaglio sul DNA. Grazie all'inattivazione di uno dei due siti nucleasici di Cas9, l'attività dell'enzima genera una rottura a singolo filamento (SSB): in presenza di un oligonucleotide donatore identico alla sequenza bersaglio ma presentante la mutazione desiderata, potrà avvenire riparazione per ricombinazione omologa e il DNA riparato avrà quindi la modifica di interesse.

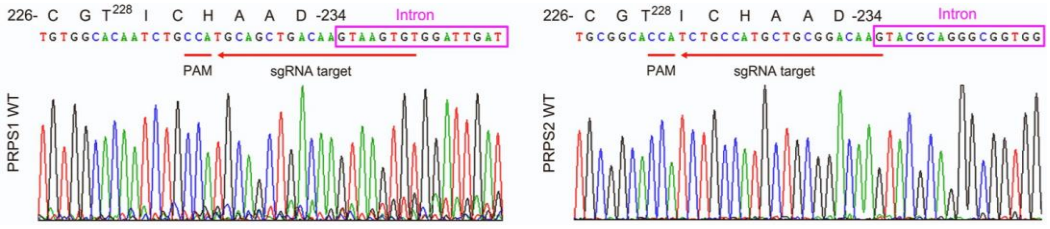

Figura 3. Regione target di appaiamento del sgRNA nei geni di PRPS1 WT e di PRPS2 WT. [10]

Cellule FHs 74 Int al 60% di confluenza sono state co-trasfettate con:

- Un oligonucleotide donatore, usato come templato per introdurre le mutazioni);
- Un vettore capace di co-esprimere un sgRNA bersagliante i geni per PRPS1 e PRSP2 e una hSpCas9 (humanized *Streptococcus pyogenes* Cas9) *wild type* marcata con GFP.

Un giorno dopo la trasfezione, le cellule sono state trattate con tripsina e diluite. Solo le cellule GFP+ sono poi state oggetto di estrazione di DNA genomico, in quanto uniche cellule esprimenti la nucleasi hSpCas9. È stata poi comunque effettuata una genotipizzazione sequenziando prodotti di PCR amplificati tramite primers vicino all'area mutata, per ottenere la certezza dell'avvenuta mutazione nel genoma della cellula.

2.8 Misurazione delle concentrazioni intracellulari di dNTPs e PRPP

Il pool dei deossiribonucleotidi è stato estratto usando acetonitrile/acqua/acido formico 90/9/1 (v/v/v), e PRPP è stato estratto con un tampone etanolo/10 mmol/l HEPES 75/25 (v/v). I dNTPs sono stati poi purificati tramite un sistema di cromatografia liquida composto da una colonna per HPLC *Thermo Hypercarb*. I dati sono stati acquisiti tramite spettrometria di massa ad alta risoluzione (HRMS), dove l'integrazione dei picchi e il calcolo delle aree sottese sono stati effettuati dal software *Thermo Trace Finder*.

2.9 Saggio di proliferazione cellulare con BrdU

[8] La 5-bromo-2'-deossiuridina (BrdU) è un analogo della timidina, da cui differisce per il fatto di avere in posizione 5 un atomo di bromo al posto di un gruppo metile. BrdU compete con la timidina per l'incorporazione nel DNA durante la fase S del ciclo cellulare, per questo viene usata come marcatore della sintesi di DNA e quindi anche di attiva proliferazione cellulare. Dopo l'incorporazione, BrdU è rilevata con metodi immunochimici.

Come step preparatorio è previsto un trattamento denaturante per il DNA (sotto forma di enzimi nucleasici o calore), necessario per permettere agli anticorpi di accedere alla BrdU incorporata nel DNA a singolo filamento. In seguito all'incorporazione, BrdU viene rilevata tramite metodi immunochimici: i campioni infatti sono stati fissati e incubati con anticorpi monoclonali anti-BrdU. Viene in seguito effettuata l'incubazione con un anticorpo secondario, il quale è associato ad un enzima che in seguito all'interazione con un substrato fornito dallo sperimentatore determina una reazione colorimetrica.

2.10 Saggio clonogenico di sopravvivenza

Il saggio clonogenico è un saggio in vitro basato sulla capacità di una singola cellula di crescere e formare una colonia, intesa come gruppo di almeno 50 cellule. Questo saggio viene usato per determinare l'inibizione delle capacità riproduttive di una cellula dopo trattamento con IR.

24 ore dopo l'irraggiamento, 100 cellule sono state seminate in uno dei sei pozzetti di una piastra. Dopo 14 giorni di coltura, le cellule sono state fissate e colorate con una soluzione 0.5% cristal violetto e 20% etanolo. Sono stati contati solo i cloni formati da più di 50 cellule.

2.11 Analisi dell'efficienza di riparazione NHEJ e HR

Si è voluto studiare l'impatto della fosforilazione di PRPS1/2 in T228 (e la sua conseguente attivazione) sull'efficienza di riparazione di DSBs riguardante i *pathways* NHEJ e HR.

In cellule HOK e FHs 74 Int è stato inserito il locus artificiale DR-GFP (*Direct Repeats – GFP*). Il locus contiene due *repeats* per GFP, una a monte detta "SceGFP" e una a valle detta "iGFP". SceGFP non è funzionante, a causa del rimpiazzo di 11 bp della sequenza per GFP con 18 bp costituenti il sito di riconoscimento per l'endonucleasi I-SceI. SceGFP non codifica quindi GFP ma può essere tagliato da I-SceI. L'espressione di I-SceI genera un DSB, che potrà quindi essere riparato tramite il *pathway* NHEJ oppure il *pathway* HR. Dopo la riparazione, viene effettuata una reazione di PCR sfruttando le sequenze di attacco dei *primers* che fiancheggiano il sito I-SceI. (Vedi *figura 4*).

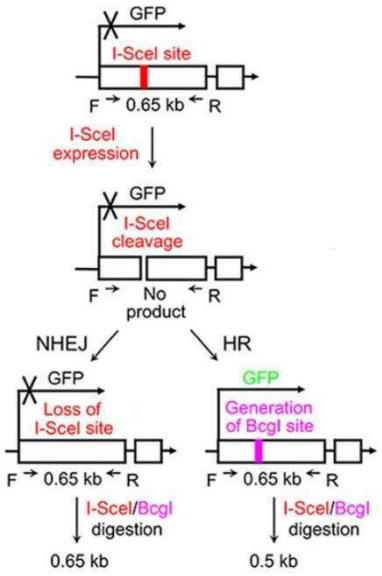

Figura 4. Locus DR-GFP e prodotti di riparazione tramite NHEJ e HR. [10]

La riparazione tramite NHEJ risulta in un prodotto di PCR da 0.65 kb, resistente alla digestione sia con I-SceI che con BcgI (dato che il sito per I-SceI viene rimosso dalla precedente digestione).

La riparazione tramite HR, oltre a ripristinare l'espressione di GFP, porta alla comparsa di un sito di taglio per BcgI e alla generazione di un prodotto di PCR da 0.5 kb. Il motivo per cui la riparazione tramite HR ripristina l'espressione di una GFP funzionante risiede nel fatto che la *repeat* a valle, ossia iGFP, può essere usata come templato per riparare il danno grazie all'omologia di sequenza con SceGFP. Se ciò avviene, viene originata una sequenza funzionante per GFP e la cellula diventa GFP+, acquisendo una fluorescenza che può essere verificata tramite citofluorimetria a flusso.

Per quanto riguarda il protocollo sperimentale seguito dagli autori, cellule contenenti il locus DR-GFP sono state transfettate in modo transiente con un vettore esprimente I-SceI. Dopo 36 ore le cellule sono state trattate con inibitori della riparazione del DNA per consentire l'accumulo di DSBs mediati da I-SceI. In seguito sono state trattate con radiazioni ionizzanti. Per l'analisi della riparazione NHEJ, le cellule sono state incubate con lovastatina per 24 ore prima

dell'irraggiamento, sincronizzando le cellule in fase G1 del ciclo cellulare. Uguali quantità di prodotti di PCR sono state soggette a digestione con I-SceI e BcgI.

Per la misurazione della riparazione NHEJ è stato calcolato il rapporto tra la quantità di ampliconi da 0.65 kb e da 0.5 kb. Per la misurazione della riparazione HR, 72 ore dopo l'irraggiamento le cellule sono state colorate con Hoechst (che lega il DNA in nuclei di cellule vive) ed è stata calcolata la percentuale di cellule GFP+ come rapporto tra cellule GFP+/nucleo Hoechst+.

Quindi, tra cellule che esprimono PRPS1/2 *wild type* e cellule con mutanti di PRPS1/2 T228A o S16A, un'eventuale differenza nell'efficienza di riparazione tramite NHEJ o HR si traduce rispettivamente in una diversa quantità di ampliconi da 0.65 kb o di cellule GFP+. Infatti, se la riparazione del DSB non è avvenuta, non ci sarà alcun prodotto di PCR e la cellula non presenterà fluorescenza.

2.12 Analisi della sintesi di DNA *gap-filling*

La sintesi di DNA *gap-filling* mediata da DNA polimerasi è frequentemente richiesta dai *pathway* NHEJ e HR dopo danno al DNA e la velocità della reazione di polimerizzazione può essere influenzata dalle concentrazioni cellulari di dNTPs. La disponibilità di dNTPs può quindi essere indirettamente correlata alla possibilità di eseguire sintesi *gap-filling,* che diventa oggetto di misurazione proprio in quanto processo dipendente dalle dimensioni del pool di nucleotidi. L'efficienza di sintesi *gap-filling* è stata misurata in cellule WT e in cellule con PRPS1/2 mutate in T228 (quindi non fosforilabili da TBK1) o in S16 (quindi non fosforilabili da ATM, e di conseguenza nemmeno da TBK1).

(Vedi *figura 5*). Dopo il trattamento con IR, sono stati transfettati nelle cellule dei *duplex* di DNA (marcati con biotina) contenenti un gap da 4 nt e usati come costrutto *reporter*. Tali *duplex* sono quindi stati oggetto di sintesi *gap-filling* in modo proporzionale alle capacità della cellula e successivamente recuperati tramite *beads* con streptavidina. Sono stati poi sottoposti ad un saggio *gap-filling* in vitro con [^{32}P]-dNTPs e successivamente la radioattività dei costrutti è stata misurata tramite scintillamento.

Dato che i dNTPs radioattivi potevano solo essere incorporati in duplex di DNA non riparati dalle cellule oppure in duplex parzialmente riparati, la radioattività dei duplex è stata usata come misura indiretta della capacità di effettuare sintesi *gap-filling* delle cellule.

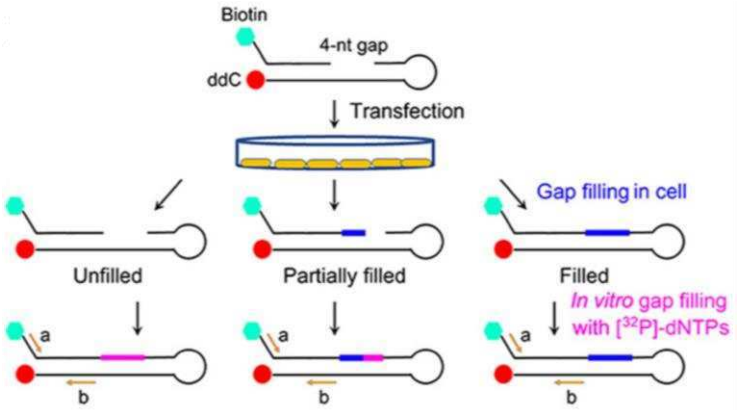

Figura 5. Schema della procedura per l'analisi della sintesi di DNA *gap-filling*. [10]

Capitolo 3 – Risultati e discussione

3.1 Radiazioni ionizzanti inducono la fosforilazione e conseguente attivazione di PRPS1/2 tramite TBK1

Gli autori della ricerca qui presentata hanno osservato un aumento delle concentrazioni di dNTPs dopo il trattamento con IR in cellule HUVECs, HOKs e FHs 74 Int. Il primo obiettivo degli autori è stato quello di capire se tale *pool* di precursori del DNA derivasse dalla via di sintesi glicolitica (vedi *figura 2*). Questo è stato confermato incubando le cellule con [^{13}C]-glucosio e trattandole successivamente con radiazioni ionizzanti: tale radioisotopo era infatti incorporato nel pool aumentato di dNTPs. Non sono stati misurati incrementi nelle concentrazioni di ribosio-5-fosfato (R5P), suggerendo come l'aumentata sintesi di dNTPs non fosse dovuta alla produzione di R5P attraverso la via PPP (vedi *figura 2*). È stato però osservato un significativo aumento nelle concentrazioni di PRPP, molecola sintetizzata a partire da R5P grazie agli enzimi PRPS1 e PRPS2. Analisi di immunoblotting non hanno rilevato differenze nell'espressione di PRPS1/2 tra cellule irraggiate e cellule non irraggiate, mentre è stato misurato un aumento della loro attività enzimatica in funzione del tempo dopo l'irraggiamento e in risposta a differenti dosi di IR (vedi *figura 6*).

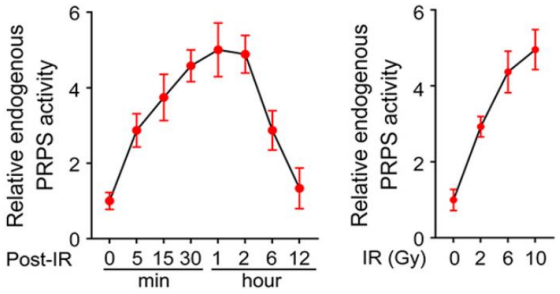

Figura 6. Quantificazione dell'attività di PRPS in funzione del tempo successivo all'irraggiamento e in funzione dell'intensità della radiazione ionizzante. [10]

Per capire il meccanismo alla base dell'aumento in attività di PRPS1/2 dopo trattamento delle cellule con IR, PRPS1 espressa con FLAG-tag è stata immunoprecipitata da estratti di cellule FHs 74 Int irraggiate: la chinasi TBK1 è stata rilevata negli immunoprecipitati di PRPS1 tramite analisi di spettrometria di massa.

Gli autori hanno quindi ipotizzato che l'elevata attività di PRPS1/2 dipenda dall'interazione con TBK1, per questo hanno effettuato un saggio di attività chinasica in vitro tra TBK1 e PRPS1 seguito da una cromatografia liquida e da analisi di spettrometria di massa che hanno consentito di identificare una fosforilazione in posizione T228. Gli stessi risultati sono stati confermati anche in PRPS2 sottoposta allo stesso trattamento (vedi *figura 7*).

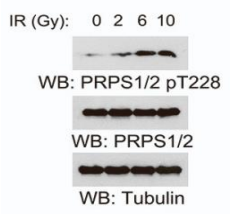

Figura 7. Western blot contro PRPS1/2 fosforilata in T228 e contro PRPS1/2 in funzione dell'intensità della radiazione ionizzante. [10]

Ulteriori analisi hanno dimostrato come la fosforilazione in T228 in PRPS1/2 risulti proporzionale alla dose di IR usata per trattare le cellule, e come venga ridotta se TBK1 viene silenziato tramite shRNA o quando viene espressa la forma non fosforilabile (mutazione T228A) di PRPS1/2.

È stato poi dimostrato che TBK1 viene attivata, dopo trattamento delle cellule con radiazioni ionizzanti, da una fosforilazione in posizione S172. Tale modifica non è invece presente in proteine TBK1 purificate da cellule non irraggiate.

Infine, è stato chiarito come sia proprio la fosforilazione in T228 ad aumentare l'attività di PRPS1/2. Come si può osservare in *figura* 8 solo PRPS1/2 WT viene attivata in seguito a trattamento delle cellule con IR, mentre nel mutante T228A l'attività è significativamente diminuita in tutte le linee cellulari analizzate.

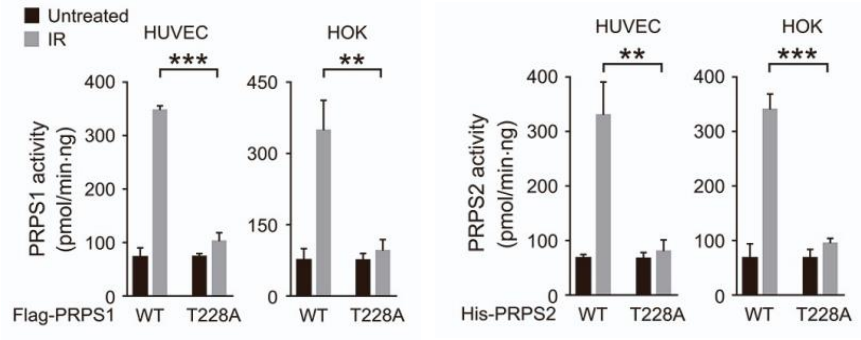

Figura 8. Confronto delle attività enzimatiche di proteine PRPS1/2 WT e mutanti non fosforilabili T228A in cellule HUVEC e HOC non trattate e trattate con radiazioni ionizzanti. [10]

3.2 Il *pathway* cGAS/STING è necessario per l'attivazione di PRPS1/2

Gli autori hanno poi dimostrato come il *pathway* cGAS-STING sia necessario per l'attivazione di PRPS1/2 da parte di TBK1. Il *pathway* cGAS-STING viene attivato quando l'enzima cGAS, presentante un *DNA binding site*, rileva DNA citosolico e catalizza la sintesi del secondo messaggero cGAMP, che interagisce infine con STING. L'interazione permette a STING di reclutare e attivare la chinasi TBK1. L'inattivazione del *pathway* cGAS/STING tramite shRNAs o l'inibizione di STING tramite due antagonisti (H-151 e C-170) hanno largamente ridotto la fosforilazione di PRPS1/2 in posizione T228 in cellule irradiate, dimostrando come l'attivazione degli enzimi PRPS dipenda dalla presenza di DNA citosolico, generato dai danni al DNA indotti da radiazioni ionizzanti.

Gli autori di questo studio hanno voluto dimostrare l'importanza di cGAS nell'attivazione di PRPS1/2 mediante un altro approccio sperimentale, andando quindi a valutare l'attività di PRPS associata ad una riduzione delle concentrazioni di frammenti di DNA citosolico. In cellule FHs 74 Int è stato sovra-espresso TREX1, una DNA esonucleasi 3'-5', per ridurre il contenuto di DNA citosolico causato da danni da IR. Come si vede in *figura* 9, un'aumentata espressione di TREX1 è associata ad una diminuzione dell'attività di enzimi PRPS.

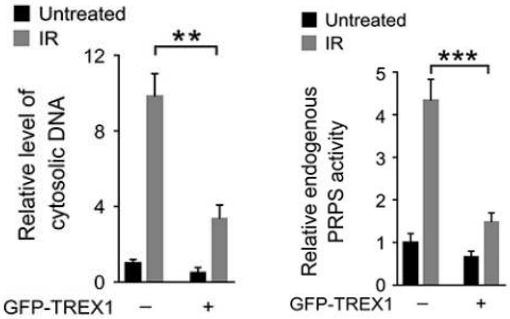

Figura 9. Contenuto di DNA citosolico e attività degli enzimi PRPS in cellule irraggiate e non, in funzione dell'over-espressione della nucleasi TREX1. [10]

3.3 La fosforilazione di PRPS1/2 in T228 da parte di TBK1 interferisce con l'inibizione allosterica da nucleotidi

L'attività enzimatica di PRPS 1 e 2 viene inibita da nucleotidi come adenosina difosfato (ADP), adenosina monofosfato (AMP), inosina monofosfato (IMP) e guanosina monofosfato (GMP), tramite la stessa tasca allosterica. La struttura di PRPS1 in uomo mostra come il residuo T228 sia localizzato proprio all'interno di tale tasca, suggerendo come la fosforilazione di questa treonina possa avere effetti sulla regolazione allosterica di PRPS1/2 (vedi *figura 10*).

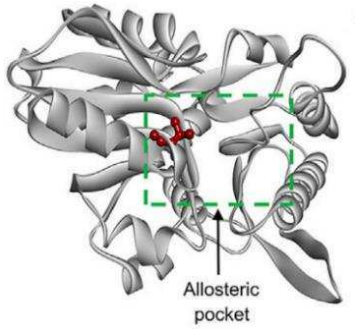

Figura 10. Rappresentazione della tasca allosterica e del residuo T228 in PRPS1 di uomo. [10]

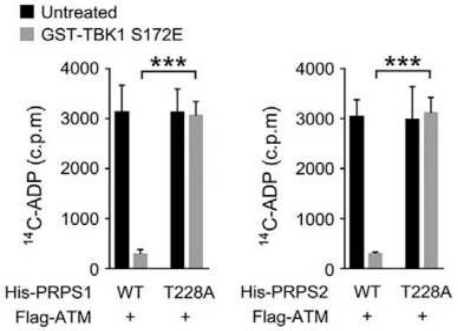

Figura 11. Associazione di [14C]-ADP con PRPS1 e PRPS2 WT e mutate T228A, quando non trattate con TBK1 o quando trattate con TBK1 mutante privo di attività chinasica. [10]

Sono stati condotti degli esperimenti per valutare l'associazione con ADP sia negli enzimi PRPS1 e PRPS2 *wild type*, che nei loro mutanti T228A (non fosforilabili). Le analisi sono state effettuate anche dopo il trattamento di PRPS1/2 con una versione mutante di TBK1, attiva in modo costitutivo senza attivazione della cascata cGAMP-STING. I risultati mostrano un'interazione con ADP molto ridotta per PRPS1/2 *wild type* dopo il trattamento con la chinasi TBK1 (vedi *figura 11*); risultati coerenti sono stati ottenuti incubando PRPS1/2 con altri inibitori allosterici, inclusi IMP, GMP e AMP. È stato quindi dimostrato come la fosforilazione in T228 di PRPS vada a diminuirne l'inibizione allosterica da nucleotidi, impedendo loro l'accesso alla tasca allosterica.

3.4 La fosforilazione di PRPS1/2 in S16 mediata da ATM è necessaria alla successiva interazione con TBK1

Il trattamento delle cellule con un inibitore di ATM, importante sensore di DSBs, ha ridotto notevolmente l'associazione di PRPS1/2 con TBK1, suggerendo che ATM sia necessaria per permettere l'interazione tra le due proteine. Diverse analisi hanno mostrato come ATM tenda ad accumularsi nel citosol dopo trattamento delle cellule con IR e un saggio di attività chinasica in vitro ha dimostrato che ATM può fosforilare proteine ricombinanti PRPS1/2. Studiando le sequenze delle proteine PRPS1 e PRPS2 sono stati individuati due residui di serina potenzialmente fosforilabili da parte di ATM: S16 ed S132. Tuttavia, solo la mutazione di S16, residuo conservato tra PRPS1 e PRPS2, impedisce la fosforilazione da parte di ATM e la deplezione di ATM tramite shRNA riduce notevolmente il grado di fosforilazione di PRPS1/2 in posizione S16 in cellule FHs 74 Int, HUVECs e HOKs irraggiate. Inoltre, la fosforilazione in S16 di PRPS1/2 è una modificazione post-traduzionale dinamica, ossia risponde al trattamento con radiazioni ionizzanti in funzione dell'intensità della radiazione e della durata del trattamento stesso. La fosforilazione in S16 correla con il pattern di attività di PRPS1/2, con la fosforilazione di PRPS1/2 in T228 da parte di TBK1 e anche con la fosforilazione di ATM in S1981 (modifica che attiva la chinasi ATM e che viene considerata un marcatore di danno al DNA) (vedi *figura 12*).

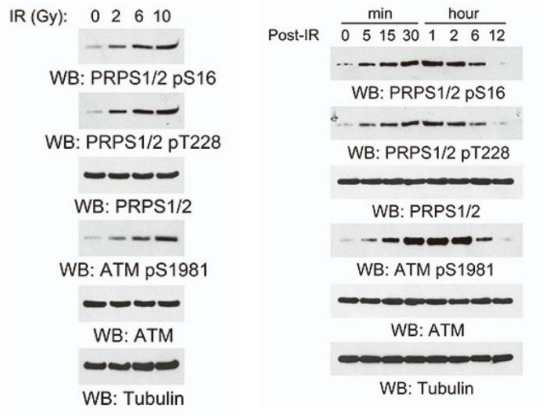

Figura 12. Western blot contro PRPS1/2 pS16, PRPS1/2 pT228, PRPS1/2, ATM pS1981, ATM, in funzione all'intensità di radiazioni ionizzanti e in funzione al tempo dopo il trattamento. [10]

3.5 La fosforilazione di PRPS1/2 in T228 promuove la sintesi di DNA e la proliferazione cellulare dopo trattamento con IR

Per esaminare l'impatto della fosforilazione di PRPS1/2 in T228 effettuata da TBK1 sulla sintesi di DNA, è stata utilizzata la metodologia descritta nel paragrafo 2.11. Il saggio ha mostrato come il *pathway* NHEJ e il *pathway* HR siano fortemente promossi in cellule con PRPS1/2 *wild type* fosforilate al sito T228 dopo irraggiamento, rispetto a cellule trattate con IR ma con PRPS1/2 mutanti nei siti T228A o S16A.

L'analisi della sintesi di DNA *gap-filling* ha rivelato come l'efficienza di riparazione risulti superiore in cellule irraggiate che esprimono PRPS1/2 *wild type* rispetto alle stesse cellule con PRPS1/2 mutante T228A o S16A. Interessante notare inoltre come la riparazione migliori anche nelle cellule mutanti per PRPS1/2 se trattate con dNTPs esogeni (vedi *figura 13*).

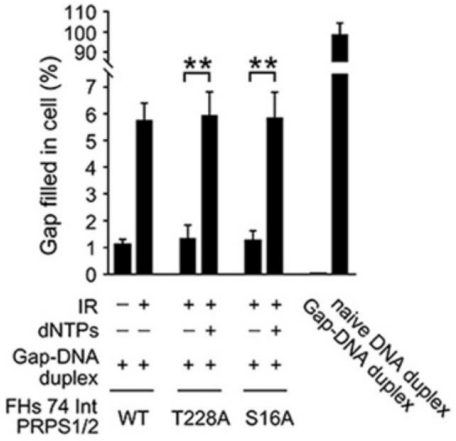

Figura 13. Percentuale di sintesi *gap-filling* in cellule con PRPS1/2 wild type e mutanti T228A e S16A. Viene anche mostrato il risultato del "salvataggio" della sintesi tramite aggiunta di dNTPs esogeni. [10]

L'ultima analisi effettuata dagli autori riguarda invece la proliferazione e la sopravvivenza cellulare. Il saggio con BrdU e il saggio clonogenico hanno entrambi dimostrato come il trattamento con radiazioni ionizzanti porti ad una diminuzione della proliferazione e del tasso di sopravvivenza sia in cellule FHs 74 Int e HOKs che esprimono enzimi PRPS1/2 *wild type* che in cellule mutanti per l'enzima. Proliferazione e sopravvivenza sono però risultati notevolmente inferiori in cellule con PRPS1/2 mutata in T228A o S16A (vedi *figura 14*).

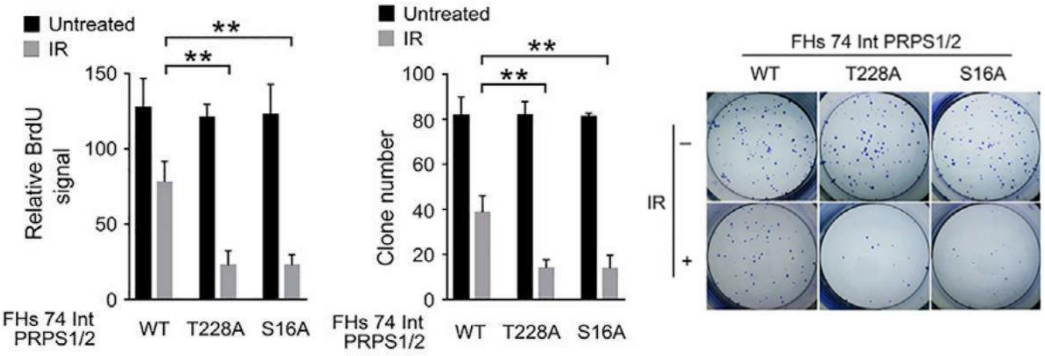

Figura 14. Nei grafici a sinistra, segnale BrdU rilevato e numero di cloni prima e dopo irraggiamento di cellule FHs 74 Int aventi PRPS1/2 wild type e mutanti T228A e S16A. A destra, colture di cellule FHs 74 Int prima e dopo trattamento con radiazioni ionizzanti. [10]

3.5 Conclusioni: la fosforilazione di PRPS1/2 in T228 promuove la sintesi di dNTPs?

Risulta evidente come i meccanismi analizzati in questo studio contribuiscano alla riparazione del DNA e al mantenimento della vitalità cellulare in cellule di mammifero sottoposte a trattamento con radiazioni ionizzanti. Gli autori di questa ricerca suggeriscono che l'aumento delle concentrazioni intracellulari di dNTP provocato dal trattamento con radiazioni ionizzanti faciliti la sintesi riparativa di

DNA, migliorando la vitalità cellulare. Secondo il modello proposto, l'aumento delle concentrazioni dei quattro nucleotidi dipende dal largo incremento della concentrazione di PRPP, intermedio sintetizzato in larga quantità grazie all'attivazione di PRPS1/2 (vedi *figura 15*).

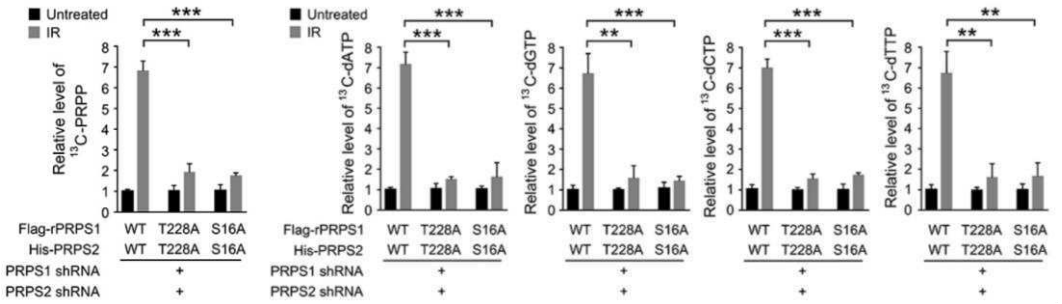

Figura 15. Concentrazioni di PRPP e di dNTPs misurate in cellule presentanti PRPS1/2 wild type e mutanti T228A e S16A. [10]

In risposta allo studio analizzato in questo elaborato è stata pubblicata una lettera di commento dal titolo "*dNTP concentrations do not increase in mammalian cells in response to DNA damage*" [3], dove Andrei Chabes e collaboratori sono in completo disaccordo con il risultato ottenuto dagli autori circa un aumento delle concentrazioni di dNTPs. La lettera discute di come gli esperimenti effettuati manchino di riproducibilità e di come il risultato ottenuto riguardo le innalzate concentrazioni di dNTPs diverga in modo notevole dalla letteratura.

L'enzima chiave nella sintesi di dNTPs, ossia RNR, non presenta in cellule di mammifero meccanismi di attivazione in risposta a danno al DNA (infatti, l'espressione della subunità p53R2, come discusso nel paragrafo 1.3, non porta ad incrementi significativi in dNTPs). Un aumento delle concentrazioni di PRPP, secondo la letteratura, non dovrebbe quindi risultare in un aumento in dNTPs, in quanto l'attività di RNR, inibita allostericamente da dATP, funge comunque da collo di bottiglia nella via di biosintesi. L'attivazione di PRPS1/2 dopo aver subito fosforilazione in T228 non giustificherebbe dunque un aumento del *pool* di dNTPs.

Le uniche limitazioni dello studio espresse dagli autori riguardano la mancanza di informazioni strutturali che spieghino nel dettaglio le conseguenze della fosforilazione di PRPS1/2 in T228. Ritengo sarebbe stato apprezzabile l'impiego di un'ulteriore metodica per confermare l'aumento delle concentrazioni dei dNTPs; ciò avrebbe conferito più robustezza ai risultati sperimentali. L'articolo analizzato da questo elaborato riporta come unica tecnica per la misurazione delle concentrazioni dei dNTPs la spettrometria di massa ad alta definizione (HRMS), tecnica di misurazione diretta. Un metodo alternativo per la misurazione delle dimensioni del *pool* di dNTPs consiste in un saggio enzimatico [9].

Tale saggio si basa sull'attività del frammento di Klenow della DNA polimerasi I, enzima dotato esclusivamente di attività DNA-polimerasica e privo di attività nucleasica. La procedura prevede l'impiego di oligonucleotidi sintetici costituiti da una sequenza di soli due nucleotidi. Questi oligo vengono usati come stampo per

sintetizzare il filamento complementare, usando per la sintesi uno specifico dNTP marcato isotopicamente e fornito in eccesso, e il pool dei dNTP estratto dalle cellule dove viene misurato un dNTP alla volta. La radioattività del costrutto ottenuto viene poi misurata mediante uno scintillatore e conferisce una misura indiretta del rapporto tra il dNTP marcato, presente nel mezzo di reazione a concentrazione nota, e il dNTP in esame. Grazie ad una curva standard preparata analizzando quantità note del dNTP da misurare è possibile quindi misurare le concentrazioni del dNTP in esame espressa in pM per milione di cellule.

Capitolo 4 – Bibliografia essenziale

[1] Pai CC, Kearsey SE. **A Critical Balance: dNTPs and the Maintenance of Genome Stability**. Genes (Basel). 2017 Jan 31;8(2):57. doi: 10.3390/genes8020057. PMID: 28146119; PMCID: PMC5333046.

[2] Nordlund P, Reichard P. **Ribonucleotide reductases**. Annu Rev Biochem. 2006;75:681-706. doi: 10.1146/annurev.biochem.75.103004.142443. PMID: 16756507.

[3] Das B, Mishra P, Pandey P, Sharma S, Chabes A. **dNTP concentrations do not increase in mammalian cells in response to DNA damage**. Cell Metab. 2022 Dec 6;34(12):1895-1896. doi: 10.1016/j.cmet.2022.11.002. PMID: 36476929.

[4] Chabes A, Georgieva B, Domkin V, Zhao X, Rothstein R, Thelander L. **Survival of DNA damage in yeast directly depends on increased dNTP levels allowed by relaxed feedback inhibition of ribonucleotide reductase**. Cell. 2003 Feb 7;112(3):391-401. doi: 10.1016/s0092-8674(03)00075-8. PMID: 12581528.

[5] Pandita TK, Lieberman HB, Lim DS, Dhar S, Zheng W, Taya Y, Kastan MB. **Ionizing radiation activates the ATM kinase throughout the cell cycle**. Oncogene. 2000 Mar 9;19(11):1386-91. doi: 10.1038/sj.onc.1203444. PMID: 10723129.

[6] Zhang M, Zou Y, Zhou X, Zhou J. **Inhibitory targeting cGAS-STING-TBK1 axis: Emerging strategies for autoimmune diseases therapy**. Front Immunol. 2022 Sep 12;13:954129. doi: 10.3389/fimmu.2022.954129. PMID: 36172373; PMCID: PMC9511411.

[7] Wang Z. **Cell Cycle Progression and Synchronization: An Overview**. Methods Mol Biol. 2022;2579:3-23. doi: 10.1007/978-1-0716-2736-5_1. PMID: 36045194.

[8] Crane AM, Bhattacharya SK. **The use of bromodeoxyuridine incorporation assays to assess corneal stem cell proliferation**. Methods Mol Biol. 2013;1014:65-70. doi: 10.1007/978-1-62703-432-6_4. PMID: 23690005.

[9] Ferraro P, Franzolin E, Pontarin G, Reichard P, Bianchi V. **Quantitation of cellular deoxynucleoside triphosphates**. Nucleic Acids Res. 2010 Apr;38(6):e85. doi: 10.1093/nar/gkp1141. Epub 2009 Dec 11. PMID: 20008099; PMCID: PMC2847218.

[10] Liu R, Li J, Shao J, Lee JH, Qiu X, Xiao Y, Zhang B, Hao Y, Li M, Chen Q. **Innate immune response orchestrates phosphoribosyl pyrophosphate synthetases to support DNA repair**. Cell Metab. 2021 Oct 5;33(10):2076-2089.e9. doi: 10.1016/j.cmet.2021.07.009. Epub 2021 Aug 2. PMID: 34343500.

Cell Metabolism

Article

Innate immune response orchestrates phosphoribosyl pyrophosphate synthetases to support DNA repair

Graphical abstract

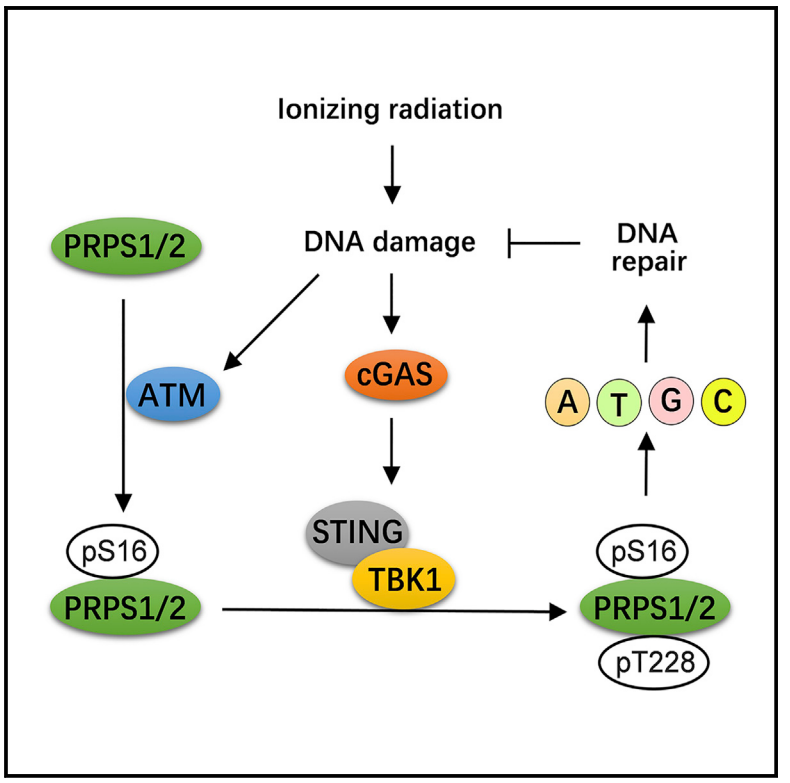

Authors

Rui Liu, Jingyi Li, Jichun Shao, ..., Yilong Hao, Mi Li, Qianming Chen

Correspondence

liurui_scu@hotmail.com (R.L.), qmchen@scu.edu.cn (Q.C.)

In brief

Liu et al. demonstrate that ionizing radiation-elicited DNA damages induce ATM and cGAS/STING/TBK1-dependent phosphorylation and activation of PRPS1/2, which accelerate the rate-limiting step during nucleotide synthesis, resulting in increased deoxyribonucleotide production, enhanced DNA repair, and elevated cell viability.

Highlights

- ATM phosphorylates PRPS1/2 in response to ionizing radiation-induced DNA damage
- TBK1 phosphorylates PRPS1/2 in an ATM- and cGAS/STING-dependent manner
- TBK1-mediated PRPS1/2 phosphorylation activates PRPS1/2
- PRPS1/2 activation promotes deoxyribonucleotide synthesis and DNA repair

Liu et al., 2021, Cell Metabolism *33*, 2076–2089
October 5, 2021
https://doi.org/10.1016/j.cmet.2021.07.009

CellPress

CellPress

Cell Metabolism

Article

Innate immune response orchestrates phosphoribosyl pyrophosphate synthetases to support DNA repair

Rui Liu,[1,8,9,*] Jingyi Li,[2,3,8] Jichun Shao,[2,8] Jong-Ho Lee,[4,7] Xuemei Qiu,[1] Yanxuan Xiao,[1] Bowen Zhang,[2] Yilong Hao,[5] Mi Li,[6] and Qianming Chen[1,*]

[1]State Key Laboratory of Oral Diseases, National Clinical Research Center for Oral Diseases, Chinese Academy of Medical Sciences Research Unit of Oral Carcinogenesis and Management, West China Hospital of Stomatology, Sichuan University, Chengdu, Sichuan 610041, China

[2]The Second Affiliated Hospital of Chengdu Medical College, China National Nuclear Corporation 416 Hospital, Chengdu, Sichuan 610051, China

[3]School of Biological Sciences and Technology, Chengdu Medical College, Chengdu 610599, China

[4]Department of Health Sciences, The Graduate School of Dong-A University, Busan 49315, Republic of Korea

[5]Key Laboratory of Oral Biomedical Research of Zhejiang Province, and the Affiliated Hospital of Stomatology, School of Stomatology, Zhejiang University School of Medicine, Hangzhou, Zhejiang 310006, China

[6]UTHealth Graduate School of Biomedical Sciences, Houston, TX 77225, USA

[7]Department of Biological Sciences, Dong-A University, Busan 49315, Republic of Korea

[8]These authors contributed equally

[9]Lead contact

*Correspondence: liurui_scu@hotmail.com (R.L.), qmchen@scu.edu.cn (Q.C.)

https://doi.org/10.1016/j.cmet.2021.07.009

SUMMARY

Ionizing radiation-induced DNA damages cause genome instability and are highly cytotoxic. Deoxyribonucleotide metabolism provides building blocks for DNA repair. Nevertheless, how deoxyribonucleotide metabolism is timely regulated to coordinate with DNA repair remains elusive. Here, we show that ionizing radiation results in TBK1-mediated phosphorylation of phosphoribosyl pyrophosphate synthetase (PRPS)1/2 at T228, thereby enhancing PRPS1/2 catalytic activity and promoting deoxyribonucleotide synthesis. DNA damage-elicited activation of cGAS/STING axis and ATM-mediated PRPS1/2 S16 phosphorylation are required for PRPS1/2 T228 phosphorylation under ionizing radiation. Furthermore, T228 phosphorylation overrides allosteric regulator-mediated effects and preserves PRPS1/2 with high activity. The expression of non-phosphorylatable PRPS1/2 mutants or inhibition of cGAS/STING axis counteracts ionizing radiation-induced PRPS1/2 activation, deoxyribonucleotide synthesis, and DNA repair, and further impairs cell viability. This study highlights a novel and important mechanism underlying an innate immune response-guided deoxyribonucleotide metabolism, which supports DNA repair.

INTRODUCTION

DNA damage caused by ionizing radiation leads to cytotoxic lesions; hence, continuous surveillance and precise DNA repair are critical for genome stability and cell viability. Double-strand break (DSB) response pathways involve three central regulators belonging to the phosphoinositide-3-kinase-related protein kinase family: ataxia-telangiectasia-mutated kinase (ATM), ATM- and Rad3-related kinase (ATR), and DNA-dependent protein kinase (DNA-PK). ATM and DNA-PK mainly respond to DSBs by initiating homologous recombination (HR) and non-homologous end joining (NHEJ)-based DNA repair (Blackford and Jackson, 2017; Huang and Shen, 2009). Deoxyribonucleotides are required for the HR pathway, which guarantees accurate repair by restoring sequence information from undamaged sister chromatid or a homologous chromosome (Li and Heyer, 2008). Although the NHEJ pathway concatenates DSBs regardless of sequence homology between the two DNA ends, DNA extension is also frequently required to fill-in single-stranded, noncompatible overhangs (Weterings and Chen, 2008). Additionally, in excision-repair pathways, which are prevalent in single-strand break (SSB) repair, a stretch of damaged DNA is removed and the resulting gap is filled in by newly synthesized DNA using the undamaged strand as a template (de Laat et al., 1999).

Deoxyribonucleotide synthesis is initiated by the pentose phosphate pathway (PPP), where glycolytic intermediates glucose-6-phosphate and fructose-6-phosphate shunt for producing ribose-5-phosphate (R5P) instead of pyruvate. A group of phosphoribosyl pyrophosphate synthetases (PRPSs) transfer the β- and γ-diphosphoryl moiety of adenosine triphosphate

(ATP) into the C1-hydroxy group of R5P to produce phosphoribosyl pyrophosphate (PRPP), which is the rate-limiting step for both subsequent *de novo* and salvage pathways for deoxyribonucleotide synthesis (Figure S1A) (Hove-Jensen, 1988; Kornberg et al., 1955). Three PRPSs have been reported thus far, which are coded by distinct genes but share very high similarity in protein sequences. PRPS1 and PRPS2 are broadly expressed in a wide spectrum of organs, while the expression of PRPS3 is restricted in the testis (Nosal et al., 1993).

Innate immunity provides the first line of defense against invading pathogens. Cyclic cGMP-AMP synthase (cGAS) is a well-established DNA sensor in innate immune responses, which associates with double-stranded cytosolic DNA to enable conformational changes, leading to enhanced production of cyclic guanosine monophosphate-adenosine monophosphate (cGAMP) from ATP and guanosine triphosphate (GTP). cGAMP functions as an endogenous second messenger by binding to the adaptor protein stimulator of interferon genes protein (STING), which recruits and activates serine/threonine protein kinase TBK1 (TBK1), thereby promoting nuclear translocation of interferon regulatory factor 3 (IRF3) and subsequent expression of type I interferon (IFN) (Burdette et al., 2011; Luo et al., 2016). cGAS-mediated DNA recognition is source or sequence independent, which renders cGAS capable of detecting self-DNA abnormally present in the cytosol, thus linking innate immunity with DNA-damage responses (Chen et al., 2016). Nevertheless, how the innate immune machinery regulates metabolic enzymes to facilitate DNA repair is still largely unknown.

In this study, we demonstrated that ATM phosphorylates PRPS1/2 S16 in response to ionizing radiation, which in turn causes PRPS1/2 T228 phosphorylation in a cGAS/STING-axis- and TBK1-dependent manner. T228 phosphorylation activates PRPS1/2 and promotes deoxyribonucleotide synthesis, thereby supporting DNA repair and cell viability.

RESULTS

Ionizing radiation induces deoxyribonucleotide synthesis and PRPS1/2 activation

First, we examined the impact of ionizing radiation on the level of cellular deoxyribonucleotides. Since epithelial cells, endothelial cells, and keratinocytes are sensitive to ionizing radiation, human FHs 74 Int normal small intestine epithelial (FHs 74 Int) cells, human normal umbilical vein endothelial cells (HUVECs), and human normal oral keratinocytes (HOKs) were exposed to ionizing radiation. We found that the levels of deoxyadenosine triphosphate (dATP), deoxyguanosine triphosphate (dGTP), deoxycytidine triphosphate (dCTP), and deoxythymidine triphosphate (dTTP) were higher 30 min after irradiation (Figures 1A and S1B) in all three cells. A similar phenomenon was also observed in these cells synchronized at G1 or G2/M phase, suggesting that the irradiation-induced expansion in deoxyribonucleotide pools was unlikely due to the increase in cell population at S phase (Figures 1B, 1C, and S1C–S1E). To determine whether the increased deoxyribonucleotide originated from glycolysis, we incubated the cells with [^{13}C]-glucose immediately after irradiation and detected an enhanced production of [^{13}C]-glucose-derived deoxyribonucleotides (Figures 1D and S1F). Of note, both the cellular level and synthesis of PRPP were increased accordingly (Figures 1E, 1F, S1G, and S1H). Considering that PRPP is required for both *de novo* and salvage synthesis pathways, we labeled FHs 74 Int cells with [$^{13}C_2$,^{15}N]-glycine or [$^{13}C_5$,$^{15}N_4$]-hypoxanthine for measuring *de novo* or salvage pathway, respectively. As expected, irradiation boosted conversion of the labeled glycine or hypoxanthine to inosine monophosphate (IMP), an intermediate for deoxyribonucleotide production, hinting at an augmentation in both pathways (Figures 1G and 1H). However, no obvious changes were detected in the level of R5P in FHs 74 Int cells, HUVECs, or HOKs (Figures 1I and S1I), suggesting that ionizing radiation-induced deoxyribonucleotide synthesis was not regulated through PPP-based R5P production.

The generation of PRPP from R5P is catalyzed by PRPS1 and PRPS2 (Hove-Jensen, 1988). However, immunoblotting with validated antibodies revealed that PRPS1 or PRPS2 was comparably expressed in untreated or irradiated cells (Figure S1J). Strikingly, increased enzymatic activities were detected in FLAG-PRPS1 or FLAG-PRPS2 immunoprecipitates from irradiated FHs 74 Int cells, HUVECs, and HOKs (Figures 1J and S1H). Further, endogenous PRPS activity changed dynamically in response to ionizing radiation at various time points after irradiation or at different doses (Figures S1L and S1M). These results suggest that ionizing radiation induces deoxyribonucleotide synthesis and PRPS1/2 activation.

TBK1-mediated PRPS1/2 phosphorylation at T228 activates PRPS1/2

To determine the mechanism underlying ionizing radiation-induced PRPS1/2 activation, FLAG-tagged PRPS1 protein was immunoprecipitated from FHs 74 Int cells after exposure to ionizing radiation, and TBK1 was found in the PRPS1 immunoprecipitates by mass spectrometry analysis (Figure S2A). The interaction of endogenous TBK1 and PRPS1 or PRPS2 was confirmed in FHs 74 Int cells, HUVECs, and HOKs (Figure 2A). TBK1 is a serine/threonine protein kinase involved in innate immune responses (Wang et al., 2014). We found that TBK1 was activated in response to ionizing radiation, as reflected by enhanced phosphorylation of TBK1 Ser (S)172 (Figure S2B) (Chen et al., 2016). An *in vitro* protein kinase assay showed that the radioactivity of FLAG-PRPS1 or PRPS2 protein, purified from ionizing radiation-treated FHs 74 Int cells, could be detected when mixed with wild-type (WT) TBK1, but not the kinase-dead TBK1 K38A mutant, in the presence of [γ-^{32}P]-ATP (Figure 2B). Notably, a constitutively active TBK1 S172E mutant mimicking S172 phosphorylation showed a greatly enhanced ability to phosphorylate PRPS1 or PRPS2 (Figure 2B). The PRPS1 protein derived from the protein phosphorylation assay was then subjected to liquid chromatography-tandem mass spectrometry (LC-MS/MS) analysis, leading to the identification of phosphorylation on PRPS1 T228 (Figure S2C), which is evolutionarily conserved for both PRPS1 and PRPS2 (Figure S2D). In line with this finding, mutation of T228 into Ala (A) abolished TBK1-mediated phosphorylation of PRPS1 or PRPS2 (Figure 2C). An antibody specifically recognizing PRPS1 pT228 and PRPS2 pT228, which shared identical flanking sequences, was prepared and validated (Figure S2E). This antibody was labeled in the figures as ‘‘PRPS1/2 pT228’’ for immunoblot analysis using cell lysates and

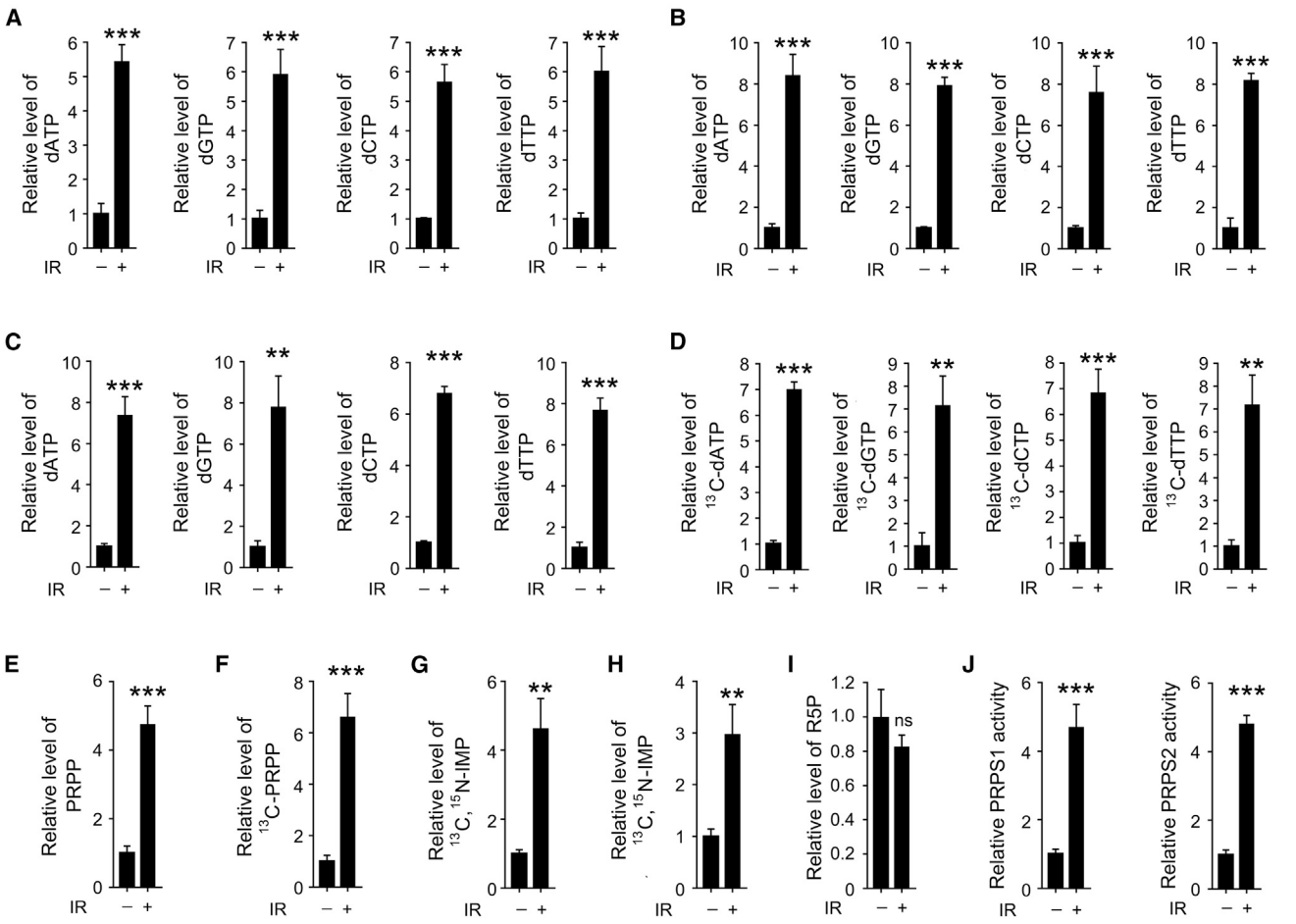

Figure 1. Ionizing radiation induces deoxyribonucleotide synthesis and PRPS1/2 activation

(A, E, and I) Indicated metabolites were measured in FHs 74 Int cells 30 min after exposure to 10 Gy ionizing radiation.

(B and C) FHs 74 Int cells that were synchronized by 20 μM lovastatin and released for 0 h (G1 phase, B) or 16 h (G2/M phase, C) were exposed to 10 Gy ionizing radiation. Indicated metabolites were measured 30 min after irradiation.

(D and F) FHs 74 Int cells were exposed to 10 Gy ionizing radiation, and then immediately incubated with $^{13}C_6$-glucose (10 mmol/L) for 30 min. Indicated ^{13}C-labeled metabolites were measured.

(G and H) FHs 74 Int cells were exposed to 10 Gy ionizing radiation, and then immediately incubated with [$^{13}C_2$,^{15}N]-glycine (0.4 mmol/L; G) or [$^{13}C_5$,$^{15}N_4$]-hypoxanthine (0.1 mmol/L; H) for 30 min. The level of labeled IMP was measured.

(J) FHs 74 Int cells with expression of His-PRPS1 or His-PRPS2 were exposed to 10-Gy ionizing radiation. An Ni-NTA pull-down assay was performed 30 min after irradiation, and PRPS activity in the precipitates was measured.

Data were normalized to the untreated group and represent the mean and SD from three independent experiments. *$p < 0.05$, **$p < 0.01$, ***$p < 0.001$. See also Figure S1.

immunohistochemical (IHC) staining using tissue samples, or as "PRPS1 pT228" or "PRPS2 pT228" for immunoblot analysis for immunoprecipitates and *in vitro* experiments. This ionizing radiation-induced T228 phosphorylation was dose dependent (Figures 2D and S2F) and could be blocked by shRNA-mediated TBK1 depletion (Figures 2F and S2G), BX795-mediated TBK1 inhibition (Figure 2F) (Pilli et al., 2012), or PRPS1/2 T228A mutation (Figures 2G and S2H). In addition, loss of two TBK1-related kinases, inducible I-kappa-B kinase epsilon (IKKε) or mitogen-activated protein kinase kinase kinase 14 (MAP3K14, also known as NIK), showed no obvious effect on PRPS1/2 T228 phosphorylation (Figure S2I). Together these results suggest that ionizing radiation induces TBK1-dependent T228 phosphorylation of PRPS1/2.

To determine whether T228 phosphorylation is required for ionizing radiation-induced PRPS1/2 activation, FLAG-PRPS1 T228A or His-PRPS2 T228A was expressed in FHs 74 Int cells, HUVECs, and HOKs. Compared with their WT counterparts, the activity of these mutants was only slightly increased in response to ionizing radiation (Figures 2H and S2J). Consistent with this finding, double-knockin expression of PRPS1 T228A and PRPS2 T228A in FHs 74 Int cells, by the CRISPR-Cas9 genome editing strategy (Figure S2K), revealed that mutated PRPS1 and PRPS2 were resistant to phosphorylation at T228 and maintained low basal activity after irradiation (Figure 2I). These results suggest that PRPS1/2 T228 phosphorylation is essential for ionizing radiation-induced PRPS1/2 activity.

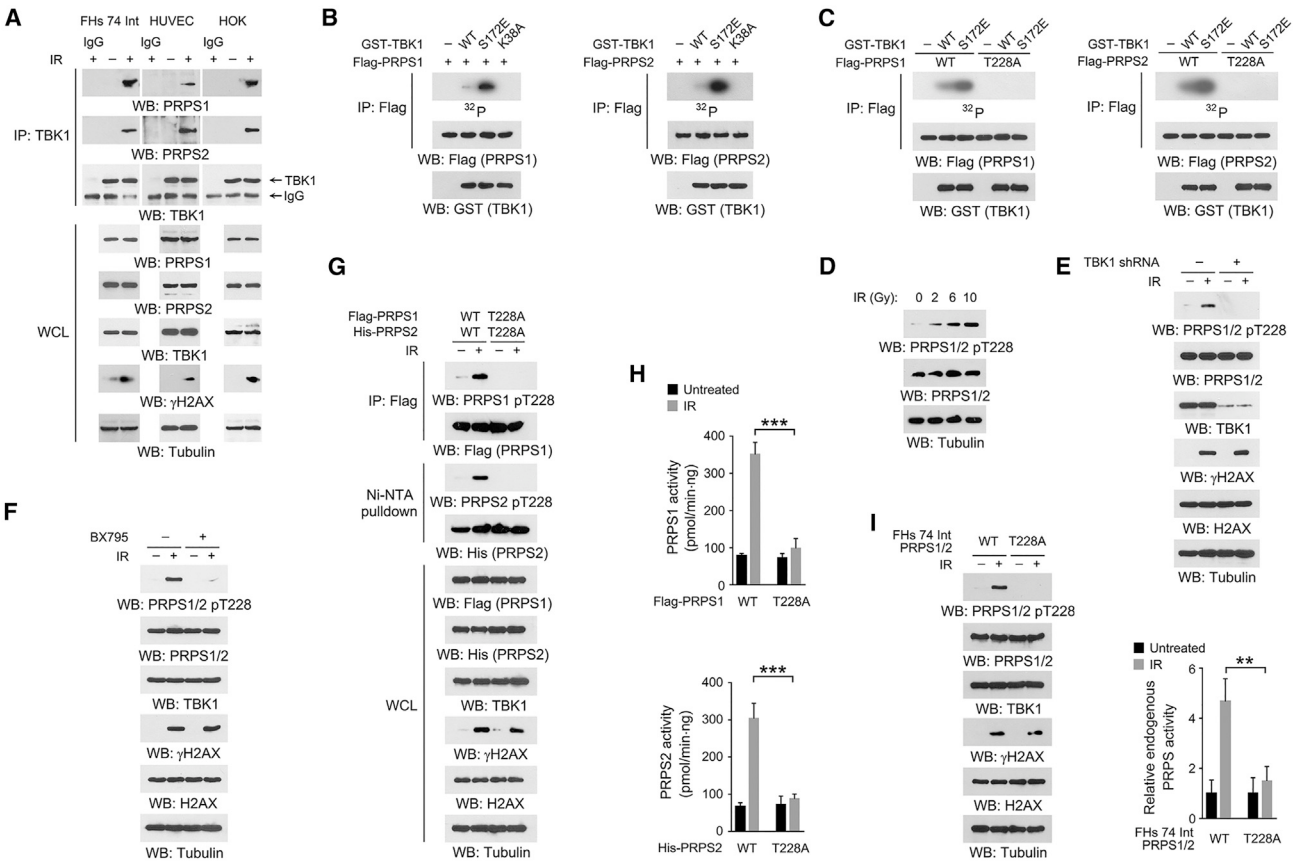

Figure 2. TBK1-mediated PRPS1/2 phosphorylation at T228 activates PRPS1/2

(A–G and I) Immunoblot analyses were performed with the indicated antibodies 1 h after irradiation unless specified.

(A) FHs 74 Int cells, HUVECs, and HOKs were exposed to 10 Gy ionizing radiation. Immunoprecipitation was performed with the indicated antibodies 1 h after irradiation. WCL, whole-cell lysate.

(B) FHs 74 Int cells with expression of FLAG-PRPS1 or FLAG-PRPS2 were exposed to 10 Gy ionizing radiation. FLAG-PRPS1 or FLAG-PRPS2 proteins were immunoprecipitated 30 min after irradiation and mixed with bacterially purified WT GST-TBK1 or indicated mutant proteins in presence of [γ-^{32}P]-ATP for an *in vitro* kinase assay.

(C) FHs 74 Int cells with expression of WT FLAG-PRPS1, WT FLAG-PRPS2, or indicated mutants were exposed to 10 Gy ionizing radiation. FLAG-tagged PRPS1/2 proteins were immunoprecipitated 30 min after irradiation and mixed with bacterially purified WT GST-TBK1 or GST-TBK1 S172E proteins in presence of [γ-^{32}P]-ATP for an *in vitro* kinase assay.

(D) FHs 74 Int cells were exposed to ionizing radiation at indicated dosages.

(E) FHs 74 Int cells with or without expression of TBK1 shRNA were exposed to 10 Gy ionizing radiation. Immunoblot analyses were performed with the indicated antibodies 1 h after irradiation.

(F) FHs 74 Int cells were pretreated with 500 nM BX795 for 2 h, and then exposed to 10 Gy ionizing radiation. Immunoblot analyses were performed with the indicated antibodies 1 h after irradiation.

(G and H) FHs 74 Int cells with expression of WT FLAG-PRPS1, FLAG-PRPS1 T228A, WT His-PRPS2, or His-PRPS2 T228A were exposed to 10 Gy ionizing radiation. Immunoprecipitation analyses with anti-FLAG M2 agarose beads and Ni-NTA agarose bead pull-down were performed 1 h after irradiation (G). PRPS activity in the precipitates was measured (H).

(I) WT FHs 74 Int cells or the FHs 74 Int cells with knockin expression of PRPS1/2 T228A were exposed to 10 Gy ionizing radiation. 1 h after irradiation, endogenous PRPS activity was measured.

Data represent the mean and SD from three independent experiments. $^{**}p < 0.01$, $^{***}p < 0.001$. See also Figure S2.

cGAS/STING axis is required for ionizing radiation-induced PRPS1/2 activation

The cGAS/STING axis, which is a crucial regulator that activates TBK1, has been linked to DNA damage (Chen et al., 2016). Therefore, we examined the effect of the cGAS/STING axis on ionizing radiation-induced PRPS1/2 T228 phosphorylation. Depletion of cGAS or STING by shRNAs (Figures 3A and S3A) or inhibition of STING by two distinct antagonists (Figure 3B), namely H-151 and C-170 (Haag et al., 2018), largely abrogated the phosphorylation of PRPS1/2 T228 in the irradiated cells. As expected, these treatments also impeded TBK1 S172 phosphorylation and IFNb expression, a downstream gene of the cGAS/STING axis (Figures 3A and 3B). cGAMP is a cGAS-produced second messenger molecule that binds with and activates STING, and it could be eliminated by ectonucleotide pyrophosphatase/phosphodiesterase 1 (ENPP1)-mediated hydrolysis

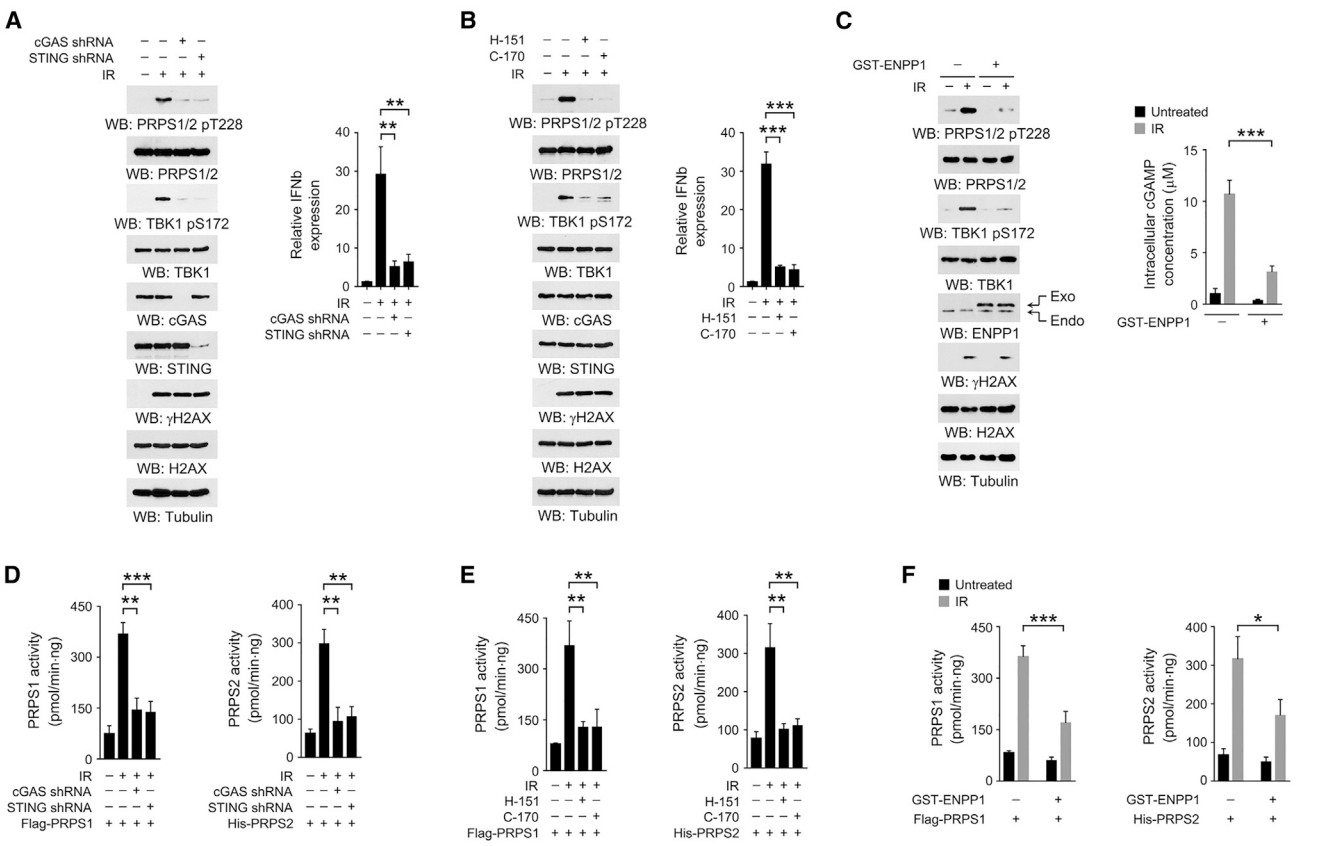

Figure 3. cGAS/STING axis is required for ionizing radiation-induced PRPS1/2 activation

(A–C) Immunoblot analyses were performed with the indicated antibodies 1 h after irradiation unless specified.

(D–F) Immunoprecipitation analyses with anti-FLAG M2 agarose beads and Ni-NTA agarose bead pull-down were performed 1 h after irradiation. PRPS activity in the precipitates was measured.

(A) FHs 74 Int cells with or without expression of cGAS or STING shRNA were exposed to 10 Gy ionizing radiation. IFNb expression was examined by qPCR 2 h after irradiation.

(B) FHs 74 Int cells were pretreated with 1 μM H-151 or 4 μM C-170 for 2 h and then exposed to 10 Gy ionizing radiation. IFNb expression was examined by qPCR 2 h after irradiation.

(C) Purified recombinant GST-ENPP1 protein (extracellular region, 98–925 aa) was delivered into FHs 74 Int cells. Cells were then exposed to 10 Gy ionizing radiation 6 h after protein delivery. Cellular cGAMP concentration was measured 30 min after irradiation.

(D) cGAS or STING-depleted FHs 74 Int cells with expression of FLAG-PRPS1 or His-PRPS2 were exposed to 10 Gy ionizing radiation.

(E) FHs 74 Int cells with expression of FLAG-PRPS1 or His-PRPS2 were pretreated with 1 μM H-151 and 4 μM C-170 for 2 h and then exposed to 10 Gy ionizing radiation.

(F) Purified recombinant GST-ENPP1 protein (extracellular region, 98–925 aa) was delivered into FHs 74 Int cells with expression of FLAG-PRPS1 or His-PRPS2, and cells were then exposed to 10 Gy ionizing radiation 6 h after protein delivery.

Data represent the mean and SD from three independent experiments. *$p < 0.05$, **$p < 0.01$, ***$p < 0.001$. See also Figure S3.

(Li et al., 2014). Indeed, delivery of a recombinant ENPP1 protein (Figure 3C) or reconstituted expression of an inactive cGAS E225A/D227A mutant (Figures S3B and S3C) in FHs 74 Int cells blocked irradiation-induced cGAMP production, TBK1 S172 phosphorylation, or PRPS1/2 T228 phosphorylation. Interestingly, these irradiation-induced effects were further reinforced by the cGAS Y215E mutation, which largely abolished cGAS translocation to the nucleus (Figures S3D and S3E) (Liu et al., 2018). As expected, ionizing radiation failed to induce similar PRPS1/2 T228 phosphorylation in the SK-MEL-5 melanoma cell line and Saos-2 sarcoma cell line, which display repressed STING expression (Figure S3F) (Chen et al., 2017; Xia et al., 2016b). Consistent with the role of the cGAS/STING axis in regulating PRPS1/2 T228 phosphorylation, loss of cGAS or STING expression, treatment with H-151 and C-170, and delivery of an ENPP1 recombinant protein abolished ionizing radiation-induced PRPS1/2 activity (Figures 3D–3F and S3G). These results suggest that the cGAS/STING axis is required for ionizing radiation-induced phosphorylation and activation of PRPS1/2 through regulating TBK1.

STING functions as a scaffold for bridging TBK1 and interferon regulatory factor 3 (IRF3) (Chen et al., 2016). However, depletion of STING did not affect FLAG-TBK1 binding with endogenous PRPS1 or PRPS2 in ionizing radiation-stimulated FHs 74 Int cells (Figure S3H). Reconstituted expression of a TBK1 S172E mutant, but not WT TBK1, was sufficient to induce PRPS1/2 T228 phosphorylation in endogenous STING and TBK1-silenced FHs 74 Int cells under ionizing radiation (Figure S3I). Further,

activation of STING alone, by C-di-GMP or cGAMP, failed to induce comparable TBK1-bound PRPS1/2 proteins, PRPS1/2 T228 phosphorylation, or PRPS1/2 activation in untreated cells, although these agonists caused overt TBK1 activation, as shown by TBK1 S172 phosphorylation and TBK1-dependent STING S366 phosphorylation (Figures S3J and S3K). Consistently, depletion of endogenous STING and reconstituted expression of WT STING, STING E260A (defective in recruiting both TBK1 and IRF3) (Shu et al., 2012), or STING S366A (functional in recruiting TBK1 but not IRF3) (Liu et al., 2015) resulted in similar amounts of PRPS1/2 proteins detected in TBK1 immunoprecipitates under ionizing radiation (Figure S3L). Compared with the regulation of IRF3, these results suggested that STING likely dose not contribute to assembling TBK1 with PRPS1/2.

Three prime repair exonuclease 1 (TREX1), a 3′-to-5′ DNA exonuclease, degrades cytosolic DNA and regulates cellular responses to radiation (Gao et al., 2015; Vanpouille-Box et al., 2017). We irradiated FHs 74 Int cells that were stably expressed GFP-TREX1 or a mock vector and revealed a decreased cytosolic DNA content in TREX1-expressed cells (Figures S3M and S3N). Consistently, the expression of TREX1 also reduced the phosphorylation of PRPS1/2 T228, TBK1 S172, STING S366, and cellular PRPS activity (Figures S3M and S3O). These data suggest that DNA fragments, which are frequently generated from ionizing radiation-elicited DNA damages, are important for PRPS1/2 activation upon ionizing radiation.

ATM-mediated phosphorylation at S16 is required for PRPS1/2 binding to TBK1

DNA-PK, ATM, and ATR are important sensors of DSBs in vertebrate cells (Blackford and Jackson, 2017). Unlike the DNA-PK inhibitor NU7441 or ATR inhibitor AZD6738, treatment with the ATM inhibitor KU55933, which largely impaired ionizing radiation-induced ATM S1981 autophosphorylation or checkpoint kinase 2 (CHK2) T68 phosphorylation (Figure S4A) (So et al., 2009; Xu et al., 2002), reduced the amount of PRPS1 or PRPS2 protein immunoprecipitated by FLAG-TBK1 (Figure 4A), suggesting that ATM is involved in regulating their association. Coimmunoprecipitation analyses further validated the binding of endogenous PRPS1 or PRPS2 with ATM (Figure 4B). An *in vitro* kinase assay showed that purified WT ATM protein phosphorylated bacterially purified PRPS1 or PRPS2 protein (Figure 4C), while such effect was not observed for a kinase-dead ATM mutant containing triple mutations of D2879A/N2884K/D2898A (Turenne et al., 2001). Analyses of the PRPS1 and PRPS2 protein sequences revealed two potential glutamine (Q)-based ATM phosphorylation consensus sequences (Taniguchi et al., 2002), $S_{16}Q$ and $S_{132}Q$. Replacement of S by A in purified PRPS1 or PRPS2 protein showed that only the mutation in $S_{16}Q$, which is shared by PRPS1 and PRPS2 and conserved among species (Figure S4B), abolished ATM-mediated phosphorylation (Figures 4D and S4C). Further, depletion of ATM by shRNA substantially abolished PRPS1/2 S16 phosphorylation in the irradiated FHs 74 Int cells, HUVECs, and HOKs, as revealed by a validated specific PRPS1/2 pS16 antibody (Figures 4E, S4D, and S4E). Cell fractionation analyses showed that cytosolic ATM accumulated upon ionizing radiation, which was consistent with previous reports (Hinz et al., 2010), while subcellular distribution of PRPS1/2 and TBK1 was not altered (Figure S4F). Although PRPS1/2 binding with TBK1 or ATM could be detected in both the cytosol and nucleus, over 80% of S16- or T228-phosphorylated PRPS1/2 was found in the cytosol (Figures S4F and S4G). These results indicate that ionizing radiation results in ATM-mediated PRPS1/2 S16 phosphorylation.

We purified FLAG-PRPS1 or His-PRPS2 protein from TBK1-depleted and ionizing radiation-stimulated cells, and found that preincubation of these proteins with calf intestinal alkaline phosphatase (CIP) abrogated their interaction with bacterial-generated GST-TBK1 protein (Figure S4H), suggesting that an irradiation-responsive phosphorylation of PRPS1 and PRPS2 might be required for recruitment of TBK1. Further, PRPS1/2 was dynamically phosphorylated at S16 in response to ionizing radiation at various time points after irradiation or at different doses (Figures S4I and S4J), which was similar to the pattern of PRPS1/2 activity (Figures S1I and S1J), PRPS1/2 T228 phosphorylation and ATM S1981 phosphorylation (Figures S4I and S4J), which is a hallmark of DNA damage (You et al., 2007). We therefore tested whether ATM-mediated PRPS1/2 S16 phosphorylation affected this binding. Indeed, HA-PRPS1 S16A or His-PRPS2 S16A expressed in FHs 74 Int cells, HUVECs, or HOKs failed to bind to TBK1 after irradiation (Figures 4F and S4K). Similar data were also obtained by double knockin of PRPS1 S16A and PRPS2 S16A in FHs 74 Int cells (Figures 4G and S4L). An *in vitro* binding assay showed that purified GST-TBK1 only interacted with ATM-phosphorylated WT His-PRPS1 or PRPS2, but not the S16A non-phosphorylatable mutants (Figure 4H). These results suggest that ATM-mediated phosphorylation is required for PRPS1/2 to bind with TBK1.

Consistently, knockin expression of PRPS1/2 S16A mutants in FHs 74 Int cells or exogenous expression of these mutants in HUVECs and HOKs counteracted ionizing radiation-induced T228 phosphorylation and activation of PRPS1/2 (Figures 4I, 4J, S4M, and S4N). However, introducing S16 phosphorylation in bacterially purified PRPS1 or PRPS2 protein, through an ATM-mediated *in vitro* kinase assay, showed limited effects on their activities (Figure S4O). Similarly, in untreated FHs 74 Int cells, the PRPS1/2 S16D mutation caused only a weak T228 phosphorylation, which could be largely enhanced by cGAMP treatment (Figure S4P), hinting that S16 phosphorylation alone is not sufficient to activate the PRPS1 or PRPS2 protein. Taken together, these results indicate that DNA damage-sensitive and ATM-dependent S16 phosphorylation facilitates PRPS1/2 binding to TBK1, leading to subsequent T228 phosphorylation and PRPS1/2 activation.

PRPS1/2 T228 phosphorylation copes with allosteric inhibitors and promotes ionizing radiation-induced deoxyribonucleotide synthesis

PRPS1 and PRPS2 are activated by phosphate (Pi) or repressed by nucleotides, including adenosine diphosphate (ADP), adenosine monophosphate (AMP), inosine monophosphate (IMP), and guanosine monophosphate (GMP), via the same allosteric pocket (Li et al., 2007). The human PRPS1 structure (PDB: 2H06) showed that T228 is located within this pocket (Figure 5A), suggesting that T228 phosphorylation may affect allosteric modulator-mediated regulation of PRPS1/2. We introduced T228 phosphorylation on bacterially purified His-PRPS1 or His-PRPS2 proteins by sequential incubation with FLAG-ATM and

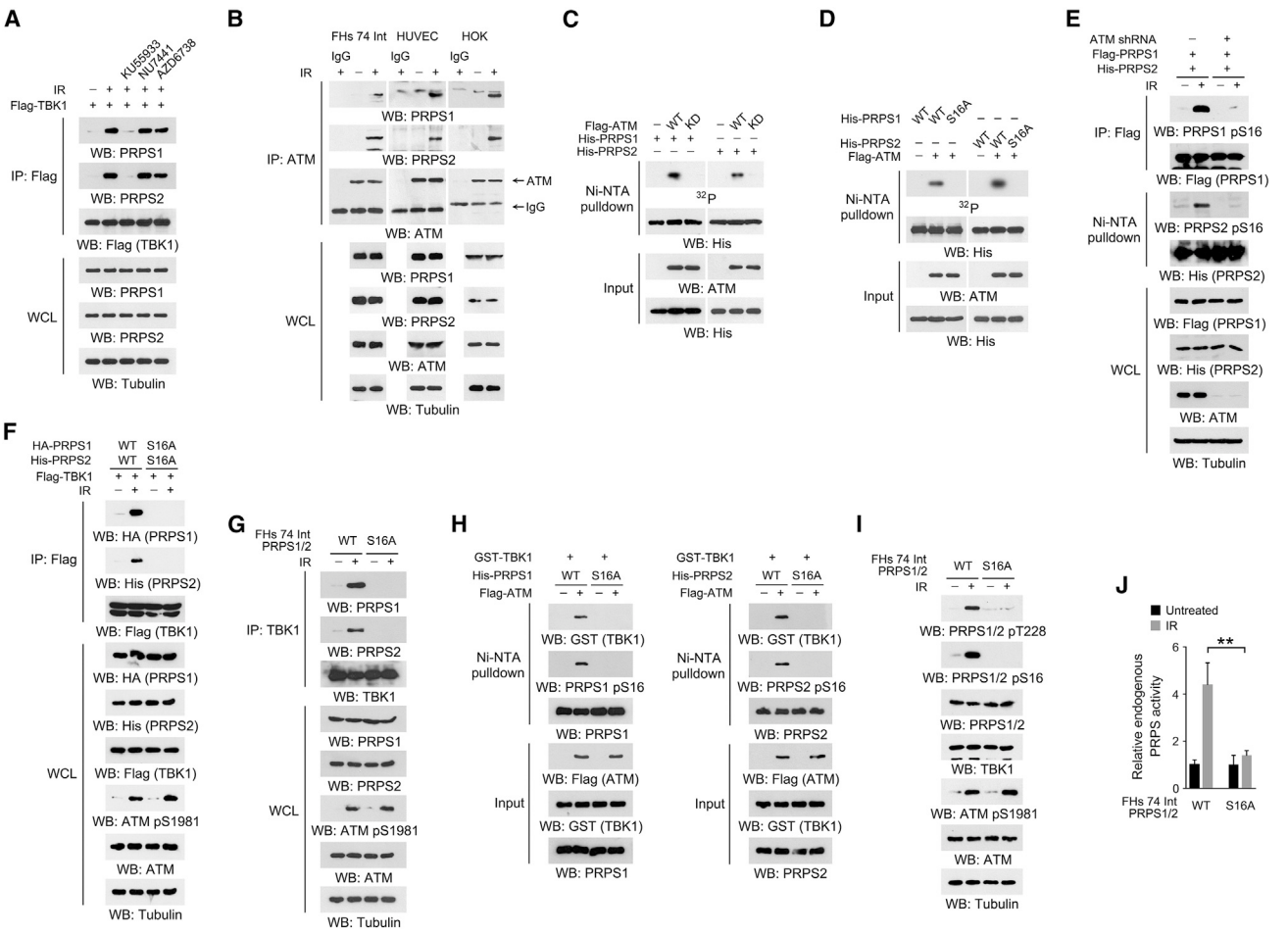

Figure 4. ATM-mediated phosphorylation at S16 is required for PRPS1/2 binding to TBK1

(A–I) Immunoblot analyses were performed with the indicated antibodies 30 min after irradiation unless specified.

(A) FHs 74 Int cells with expression of FLAG-TBK1 were pretreated with NU7441 (1 μM), KU55933 (10 μM), or AZD6738 (2 μM) for 2 h, and then exposed to 10 Gy ionizing radiation. Immunoprecipitation analyses with anti-FLAG M2 agarose beads were performed 30 min after irradiation.

(B) FHs 74 Int cells, HUVECs, and HOKs were exposed to 10 Gy ionizing radiation. Immunoprecipitation was performed with the indicated antibodies 30 min after irradiation.

(C) Bacterially purified His-PRPS1 or His-PRPS2 proteins were incubated with purified WT FLAG-ATM or kinase-dead (KD) FLAG-ATM D2879A/N2884K/D2898A proteins in the presence of [γ-^{32}P]-ATP for an *in vitro* kinase assay.

(D) Bacterially purified WT His-PRPS1, His-PRPS1 S16A, WT His-PRPS2, or His-PRPS2 S16A proteins were incubated with purified WT FLAG-ATM proteins in the presence of [γ-^{32}P]-ATP for an *in vitro* kinase assay.

(E) FHs 74 Int cells with expression of FLAG-PRPS1, His-PRPS2, or ATM shRNA were exposed to 10 Gy ionizing radiation. Immunoprecipitation analyses with anti-FLAG M2 agarose beads and Ni-NTA agarose bead pull-down were performed 30 min after irradiation.

(F) FHs 74 Int cells with expression of FLAG-TBK1, WT HA-PRPS1, HA-PRPS1 S16A, WT His-PRPS2, or His-PRPS2 S16A were exposed to 10 Gy ionizing radiation. Immunoprecipitation analyses with anti-FLAG M2 agarose beads were performed 30 min after irradiation.

(G) WT FHs 74 Int cells or FHs 74 Int cells with knockin expression of PRPS1/2 S16A were exposed to 10 Gy ionizing radiation. Immunoprecipitation analyses with the indicated antibody were performed 30 min after irradiation.

(H) Bacterially purified WT His-PRPS1, His-PRPS1 S16A, WT His-PRPS2, or His-PRPS2 S16A proteins were immobilized on beads, incubated with purified ATM protein for an *in vitro* kinase assay, washed, and incubated with purified GST-TBK1 proteins. An Ni-NTA agarose bead pull-down was performed.

(I and J) WT FHs 74 Int cells or FHs 74 Int cells with knockin expression of PRPS1/2 S16A were exposed to 10 Gy ionizing radiation. 30 min after irradiation, immunoblot analyses were performed with the indicated antibodies (I), and endogenous PRPS activity was measured (J). Data represent the mean and SD from three independent experiments. **$p < 0.01$ (J).

See also Figure S4.

GST-TBK1 S172E protein (Figure 5B). Compared with non-phosphorylatable PRPS1/2 T228A mutants, this phosphorylation largely reduced WT PRPS1 or PRPS2 protein-associated ADP (Figure 5C), suggesting that T228 phosphorylation likely obstructed the access of the allosteric pocket to ADP. Indeed, no obvious inhibitory effect of ADP was detected for T228-phosphorylated PRPS1 or PRPS2 proteins (Figure 5D); in contrast, ADP apparently counteracted phosphate-induced activation of His-PRPS1 or His-PRPS2 proteins (Figure S5A). Consistent results were obtained by treating PRPS1 or PRPS2 proteins with

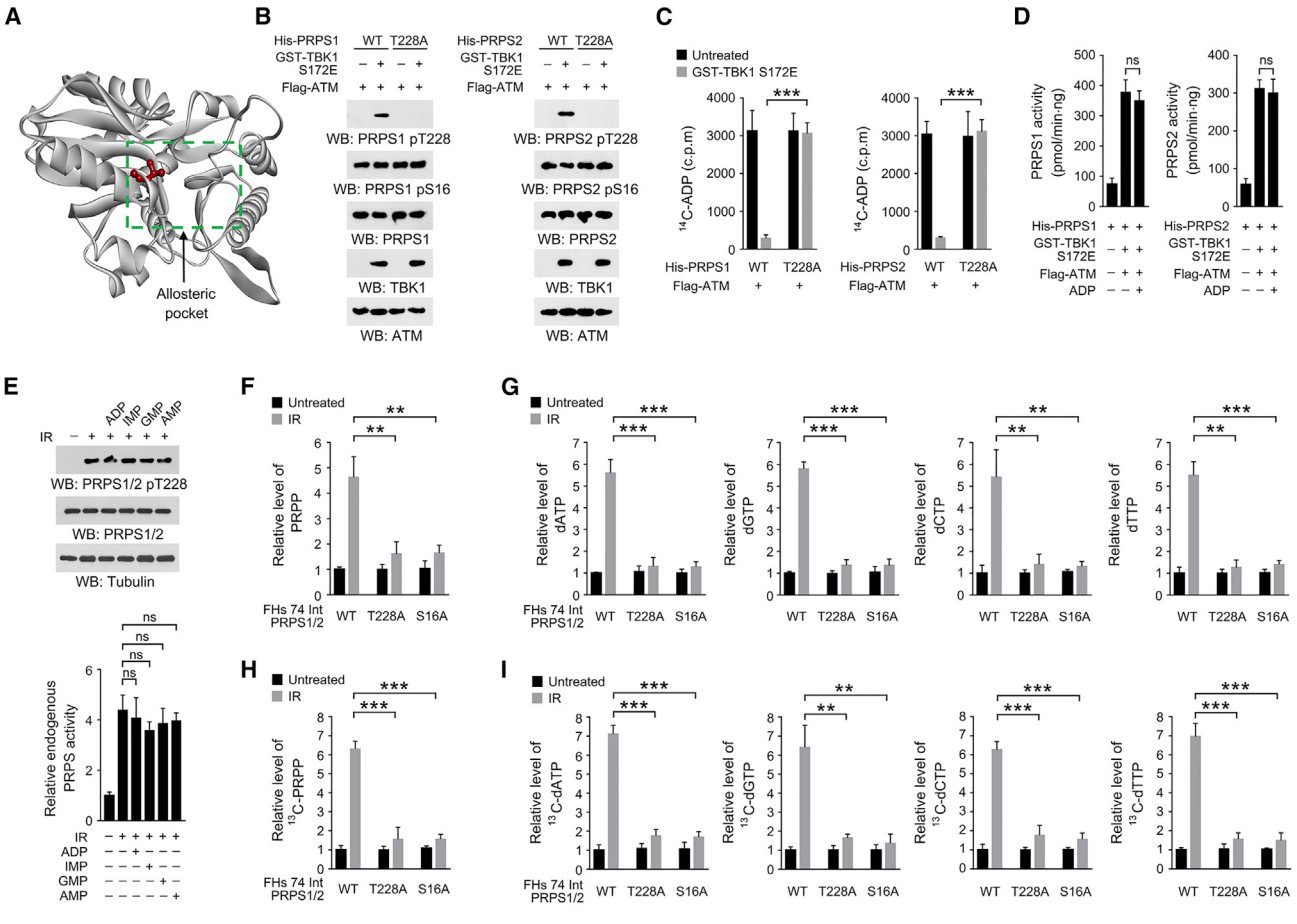

Figure 5. PRPS1/2 T228 phosphorylation copes with allosteric inhibitors and promotes ionizing radiation-induced deoxyribonucleotide synthesis

(A) Human PRPS1 structure (PDB: 2H06) shows the spatial location of T228 (side chain in red) and the allosteric pocket (boxed by green line) in a monomeric PRPS1.

(B and C) Bacterially purified WT His-PRPS1, His-PRPS1 T228A, WT His-PRPS2, or His-PRPS2 T228A proteins were immobilized on beads, incubated with purified ATM protein for an *in vitro* kinase assay, washed, incubated with purified GST-TBK1 S172E proteins for another *in vitro* kinase assay, and then washed again. Immunoblot analyses were performed with the indicated antibodies (B). The bead complexes were incubated with [^{14}C]-ADP for 12 h, washed, and the radioactivity in the beads was measured (C).

(D) Bacterially purified His-PRPS1 or His-PRPS2 proteins were sequentially subjected to ATM and TBK1 *in vitro* kinase assay, and the activity of His-PRPS1 or His-PRPS2 proteins was measured in the presence of 100 μM ADP.

(E) FHs 74 Int cells were exposed to 10 Gy ionizing radiation. One hour after irradiation, immunoblot analyses were performed with the indicated antibodies (upper panel), and endogenous PRPS activity was measured in the presence of 100 μM ADP, AMP, GMP, or AMP (bottom panel).

(F and G) WT FHs 74 Int cells or the FHs 74 Int cells with knockin expression of PRPS1/2 T228A or PRPS1/2 S16A were exposed to 10 Gy ionizing radiation. Thirty minutes after irradiation, the levels of PRPP (F) or the indicated metabolites (G) were measured.

(H and I) WT FHs 74 Int cells or the FHs 74 Int cells with knockin expression of PRPS1/2 T228A or PRPS1/2 S16A were exposed to 10 Gy ionizing radiation, and then immediately incubated with $^{13}C_6$-glucose (10 mmol/L) for 30 min. ^{13}C-labeled PRPP (H) or the indicated metabolites (I) were measured.

(C–I) Data represent the mean and SD from three independent experiments. $^{**}p < 0.01$, $^{***}p < 0.001$. ns, not significant. See also Figure S5.

other allosteric inhibitors, including IMP, GMP, and AMP (Figure S5B). Further, Pi failed to further activate T228-phosphorylated PRPS1/2 (Figure S5C). These data suggest that ionizing radiation-induced T228 phosphorylation in the allosteric pocket activates PRPS1/2 and overrides small molecule allosteric regulator-mediated effects on PRPS1/2.

To better understand the regulation of endogenous PRPS1 and PRPS2, *in vivo* stoichiometry analyses were performed, and they revealed that approximately 90% of the endogenous PRPS1 or PRPS2 proteins were phosphorylated at T228 in ionizing radiation-stimulated cells (Figure S5D). Reconstituted expression of S16A or T228A mutant of PRPS1 or PRPS2 resulted in minor changes in T228 and S16 phosphorylation, or enzymatic activity of the other PRPS (Figure S5E). Consistently, addition of ADP, AMP, IMP, or GMP had only limited effects on PRPS activity in the lysates from irradiated cells (Figure 5E). Further, in contrast to deoxyribonucleotide intermediates (Figures 1A–1H and S1B–S1H), the cellular Pi concentration was not obviously changed upon ionizing radiation (Figure S5F). Therefore, these results suggest that, despite PRPS1/2-activation-induced accumulation of

deoxyribonucleotide intermediates, T228 phosphorylation renders PRPS1/2 resistant to such inhibitory feedback and endows PRPS1/2 with constant high activities.

We next determined the effect of PRPS1/2 T228 phosphorylation in ionizing radiation-induced deoxyribonucleotide synthesis. Metabolite analyses showed that either knockin expression of PRPS1/2 T228A in FHs 74 Int cells or reconstituted expression of PRPS1/2 T228A in endogenous PRPS1/2-depleted HOKs impeded irradiation-induced production of PRPP and deoxyribonucleotides (Figures 5F, 5G, S5G, and S5H). Accordingly, the level of [^{13}C]-glucose-derived PRPP and deoxyribonucleotides was much lower in PRPS1/2 T228A-expressed cells, suggesting impaired deoxyribonucleotide synthesis (Figures 5H, 5I, S5I, and S5J). Similar results were observed in PRPS1/2 S16A-expressed cells (Figures 5F–5I and S5G–S5J). Nevertheless, ionizing radiation-induced IFNb expression was not affected by these PRPS1/2 mutations (Figures S5K and S5L). These results suggest that PRPS1/2 T228 phosphorylation promotes ionizing radiation-induced deoxyribonucleotide synthesis.

We further exposed the FHs 74 Int cells to ultraviolet light C (UVC) and methyl methanesulfonate (MMS). Indeed, these treatments also induced ATM S1981 phosphorylation, TBK1 S172 phosphorylation, PRPS1/2 S16 and T228 phosphorylation, PRPS1/2 activation, and increased deoxyribonucleotide pools (Figures S5M–S5R). Further, these UVC- or MMS-treatment-induced effects were largely abolished by knockdown of cGAS (Figures S5M–S5R), suggesting that cGAS is required for UVC- or MMS-induced deoxyribonucleotide synthesis. This is in line with recent reports showing that cGAS/STING pathway could be induced by DNA fragments generated from DNA repair (Coquel et al., 2018; Wolf et al., 2016).

TBK1-dependent PRPS1/2 phosphorylation promotes DNA repair and cell proliferation under ionizing radiation

To examine the impact of TBK1-dependent PRPS1/2 T228 phosphorylation on the NHEJ and HR pathways, endonuclease I-SceI was expressed to generate a DSB in an exogenously introduced DR-GFP locus, in the context of ionizing radiation-induced DNA damage. DNA repair through the NHEJ pathway led to a 0.65 kb PCR product that was insusceptible to both I-SceI and BcgI digestion, while HR-mediated DNA repair converted the I-SceI cutting motif into a BcgI cutting motif and restored the expression of DR-GFP (Figure S6A) (Jiang et al., 2015). As expected, I-SceI expression resulted in an apparent 0.65 kb PCR band (Figures 6A–6C) and GFP expression (Figures 6D and 6E) in WT FHs 74 Int cells, which was markedly eliminated by knockin expression of PRPS1/2 T228A or S16A mutants (Figures 6A and 6B). Given a similar I-SceI cleavage efficiency among WT and mutant groups before DNA repair (Figures 6A and 6B), the distinct amount of 0.65 kb PCR band or DR-GFP-expressing cells should have been caused by the diverse repair efficiency of NHEJ or HR pathway, respectively. Therefore, these data strongly indicated that PRPS1/2 T228 phosphorylation promoted both the NHEJ and HR pathways under ionizing radiation. Consistent with the role of TBK1 and cGAS/STING axis in regulating PRPS1/2 T228 phosphorylation, treatment with BX795 or H-151 caused the loss of the 0.65 kb PCR band and DR-GFP-positive FHs 74 Int cells (Figures 6C and 6E). Similar results were observed by the reconstituted expression of PRPS1/2 mutants or inhibition of TBK1 or STING in HOKs (Figures S6B–S6F). Notably, replenishment of cellular deoxyribonucleotide to a comparable level as that in irradiated WT cells largely rescued NHEJ and HR repair in PRPS1/2-mutated FHs 74 Int cells or HOKs (Figures 6F–6H and S6G–S6I).

Nucleotide excision repair (NER) plays important roles in the removal of UVC-induced DNA lesions (de Laat et al., 1999). We measured the effects of PRPS1/2 modifications on NER by using a DNA duplex containing a cyclobutane pyrimidine dimer (CPD; Figure S6J). As expected, PRPS1/2 S16A or T228A mutations markedly reduced the NER repair efficiency after UVC treatment, which was restored by liposome-encapsulated deoxyribonucleotide delivery (Figure S6K).

DNA polymerase-mediated gap-filling DNA synthesis is frequently required for the HR, NHEJ, and NER pathways (de Laat et al., 1999; Li and Heyer, 2008; Schrempf et al., 2021; Vincent et al., 2001; Weterings and Chen, 2008). The rate of DNA polymerase-catalyzed reactions could be affected by the cellular deoxyribonucleotide concentrations (Amie et al., 2013), which fluctuate during the cell cycle (Ferraro et al., 2010; Spyrou and Reichard, 1988). Measurement of FHs 74 Int cells, HOKs, and HUVECs revealed that cellular deoxyribonucleotide concentrations were within the 1.0–2.5 μM range at S phase, and it reduced to the 100–250 nM range at G1 or G2/M phase (Table S1), which was lower than the reported Km values (0.28–2.25 μM range) of a set of human DNA polymerases (Copeland et al., 1992; Haracska et al., 2002; Johnson et al., 2000). Further, by using a 4-nt gap-containing DNA duplex as a reporter construct (Figure S6L), we found that treatment with deoxyribonucleotide-loaded liposomes largely boosted gap-filling DNA synthesis in FHs 74 Int cells at G1 or G2/M phase (Figures S6M and S6N). Consistently, an increase in cellular deoxyribonucleotides rescued gap-filling DNA synthesis in both unsynchronized and synchronized FHs 74 Int cells with PRPS1/2 mutations (Figures S6O and S6P). Considering that more than 75% of FHs 74 Int cells, HOKs, or HUVECs were found at G1 and G2/M phase (Figure S1C), these results suggest that phosphorylation of PRPS1/2 S16 and T228 promotes gap-filling DNA synthesis in these cells.

By bromodeoxyuridine (BrdU) incorporation assay, cell proliferation assay, and clonogenic survival assay, we found that exposure to ionizing radiation decreased the proliferation or survival rate of FHs 74 Int cells and HOKs, which was further reduced by expression of PRPS1/2 T228A or S16A mutants (Figures 6I–6K and S7A–S7C). To further support this finding, WT and STING knockout mice were exposed to ionizing radiation, and small intestine, salivary glands, and neutrophil cells isolated from bone marrow tissues were analyzed with validated antibodies (Figure S7D). We found that ionizing radiation induced concurrent phosphorylation of ATM S1981 (corresponding to mouse ATM S1987), TBK1 S172, PRPS1/2 S16, and PRPS1/2 T228 (Figures 6L, S7E, and S7F). In contrast, loss of STING substantially abolished TBK1 S172 and PRPS1/2 T228 phosphorylation (Figures 6L, S7E, and S7F). As expected, exposure to ionizing irradiation decreased Ki67 staining in the intestine epithelium and salivary glands and the survival rate of neutrophils, which were further reduced in STING knockout mice

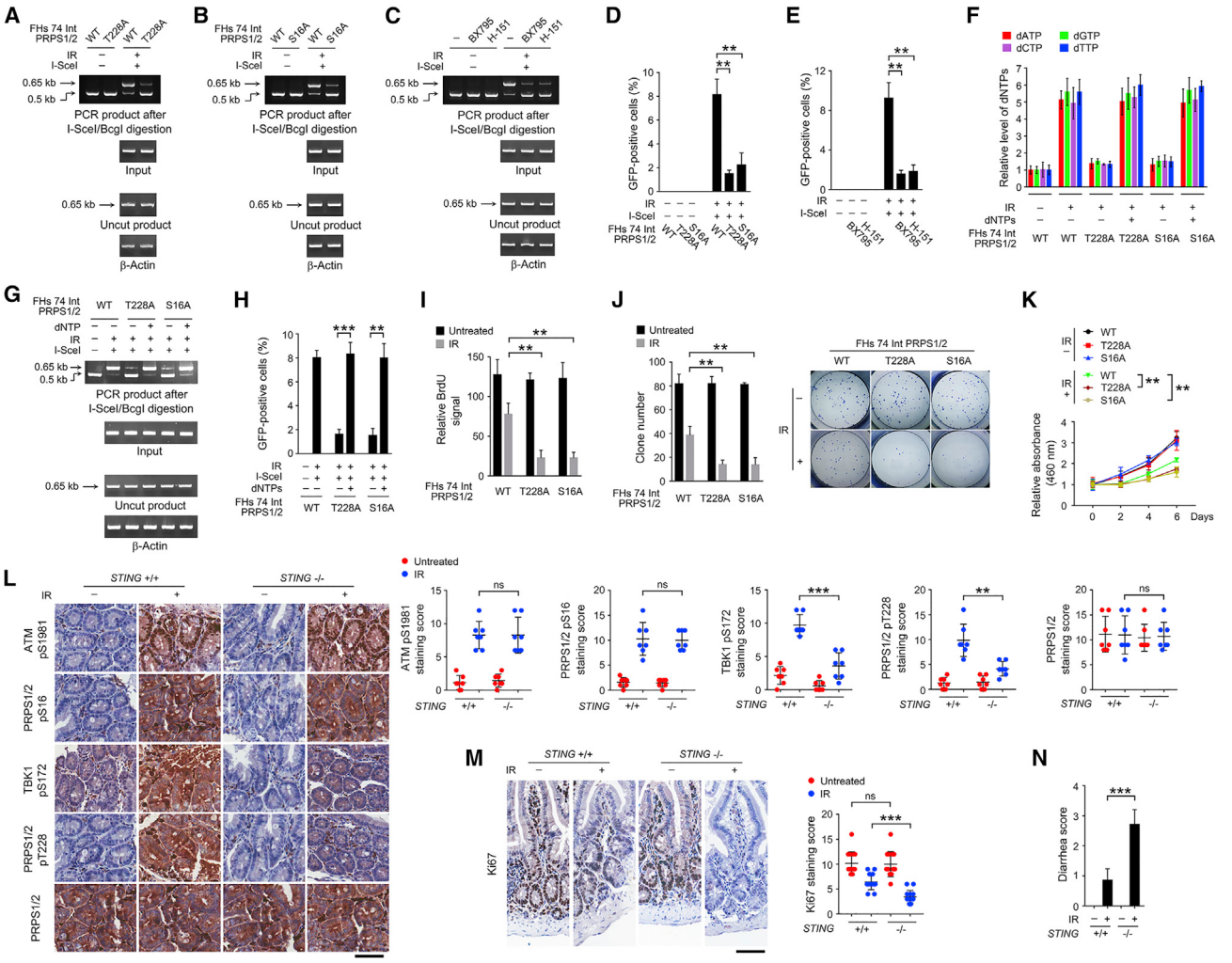

Figure 6. TBK1-dependent PRPS1/2 phosphorylation promotes DNA repair and cell proliferation under ionizing radiation

(A, B, and D) I-SceI-expressing vector was transfected into WT FHs 74 Int cells or the FHs 74 Int cells with knockin expression of PRPS1/2 T228A (A) or PRPS1/2 S16A (B), and cells were exposed to 10 Gy ionizing radiation 48 h after transfection. I-SceI cleavage efficiency was measured immediately after irradiation (A and B, bottom panel). The NHEJ pathway was measured 1 h after irradiation (A and B, upper panel). HR pathway was measured 72 h after irradiation (D).

(C and E) I-SceI-expressing vector was transfected in FHs 74 Int cells. Forty-six hours after transfection, cells were treated with 500 nM BX795 or 1 μM H-151 for 2 h and then exposed to 10 Gy ionizing radiation. I-SceI cleavage efficiency was measured immediately after irradiation (C, bottom panel). The NHEJ pathway was measured 1 h after irradiation (C, upper panel). HR pathway was measured 72 h after irradiation (E).

(F) WT FHs 74 Int cells or the FHs 74 Int cells with knockin expression of PRPS1/2 T228A or PRPS1/2 S16A were incubated with deoxyribonucleotide-loaded liposomes for 10 min and then immediately exposed to 10 Gy ionizing radiation. The cellular deoxyribonucleotide concentrations were measured.

(G and H) I-SceI-expressing vector was transfected into WT FHs 74 Int cells or the FHs 74 Int cells with knockin expression of indicated PRPS1/2 mutants. Forty-eight hours after transfection, cells were incubated with deoxyribonucleotide-loaded liposomes for 10 min, and then immediately exposed to 10 Gy ionizing radiation. The NHEJ pathway was measured 1 h after irradiation (G). HR pathway was measured 72 h after irradiation (H).

(I–K) WT FHs 74 Int cells or the FHs 74 Int cells with knockin expression of PRPS1/2 T228A or PRPS1/2 S16A were exposed to 10 Gy ionizing radiation. Cell viability was measured by BrdU incorporation assay (I), clonogenic survival assay (J), or CCK8 assay (K).

(L and M) WT or STING knockout mice were abdominally exposed to 12 Gy ionizing radiation, and intestine tissues were obtained 2 h (n = 7, L) or 72 h (n = 14, M) for IHC staining with indicated antibodies.

(N) WT or STING knockout mice were abdominally exposed to 12 Gy ionizing radiation, and diarrhea was evaluated (n = 7).

(D–F and H–N) Data represent the mean and SD from at least three independent experiments. $^{**}p < 0.01$, $^{***}p < 0.001$. ns, not significant. Scale bar, 100 μm (J); 100 μm (M). See also Figures S5 and S6 and Table S1.

(Figures 6M, S7G, and S7H). Consistently, loss of STING further enhanced abdominal irradiation-induced diarrhea in mice (Figure 6N). These results indicate that phosphorylation of PRPS1/2 S16 and T228 promotes DNA repair and cell proliferation in response to ionizing radiation.

DISCUSSION

Deoxyribonucleotides are building blocks for DNA extension during DNA repair. However, the cellular level of deoxyribonucleotides changes greatly in response to various stimuli

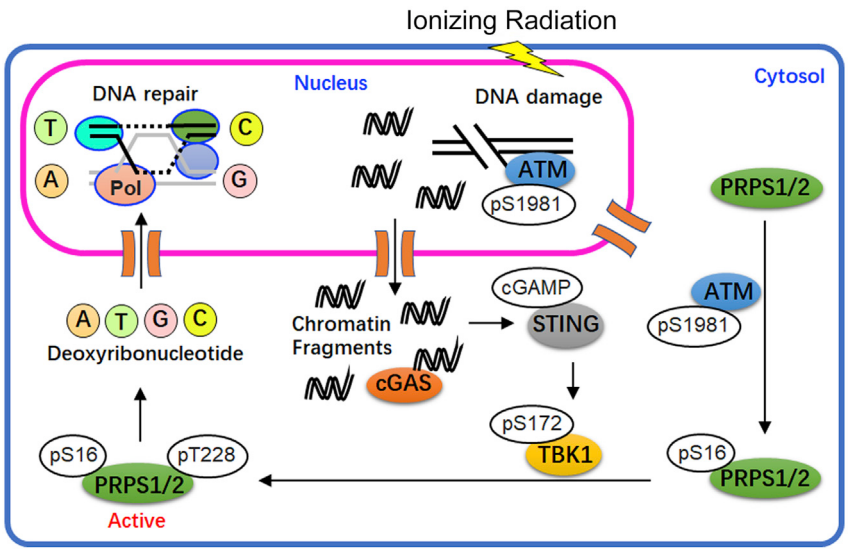

Figure 7. Model of innate immune machinery-mediated PRPS1/2 activation and deoxyribonucleotide synthesis in response to ionizing radiation

Ionizing radiation-induced DNA fragments activate cGAS/STING/TBK1 axis, leading to phosphorylation of PRPS1/2 T228, which is dependent on ATM-mediated PRPS1/2 S16 phosphorylation. T228-phosphorylated PRPS1/2 enhances deoxyribonucleotide synthesis, which facilitate DNA repair.

(Ciccia and Elledge, 2010; Ferraro et al., 2010), and an expanded deoxyribonucleotide pool has been shown to facilitate DNA repair and cell survival. Expression of p53R2, a small subunit of ribonucleotide reductase (RNR) that produces deoxyribonucleotides from ribonucleotides, was induced after ionizing radiation, and knockdown of p53R2 impeded DNA repair and enhanced DNA damage-induced apoptosis (Devlin et al., 2008). Additionally, the metabolic enzyme phosphoglycerate mutase 1 functions in maintaining the deoxyribonucleotide pool after DNA damage, which is a prerequisite for HR repair (Qu et al., 2017). In this study, we demonstrate that the levels of cellular deoxyribonucleotides are higher after exposure to ionizing radiation, which is due to enhanced PRPP synthesis from glycolysis, since more glucose-derived [^{13}C] was found in deoxyribonucleotides by tracing the metabolic flux. Importantly, inhibition of deoxyribonucleotides synthesis by PRPS1/2 mutations impaired HR, NHEJ, and NER pathways, strongly suggesting that PRPS1/2-mediated deoxyribonucleotide synthesis supports DNA repair in response to DNA damage.

Despite being best known for monitoring exogenous DNA during pathogen infection, the cGAS/STING axis can also be irritated by aberrant cytosolic self-DNA. Accumulating evidence has connected the cGAS/STING axis to ionizing radiation-elicited cellular responses, since increased cytosolic chromatin fragments are common in the context of DNA breakage (Li and Chen, 2018). Consistently, our data demonstrate that ionizing radiation evokes PRPS1/2 T228 phosphorylation and deoxyribonucleotide synthesis in a cGAS/STING-axis-dependent manner. Of note, the catalytic activity of cGAS, rather than its nuclear translocation, was required for these ionizing-radiation-mediated effects. Further, our data also show that an ionizing radiation-responsive and ATM-dependent PRPS1/2 S16 phosphorylation is prerequisite for PRPS1/2 T228 phosphorylation because S16 phosphorylation primes PRPS1/2 binding to TBK1. Therefore, this sequential phosphorylation mechanism selectively insures PRPS1/2 activation in response to DNA damage.

Nevertheless, it is still necessary to clarify the molecular requirements and contexts that define how cells coopt the cGAS/STING pathway to respond to DNA damage. For instance, a portion of cGAS was found to be translocated to DNA-damage sites and inhibit DNA repair by directly binding with DNA repair proteins (Liu et al., 2018). Short-term treatment with etoposide, a topoisomerase II inhibitor, activates IFNb expression via a non-canonical cGAS-independent mechanism, with minor activation of STING and TBK1 (Dunphy et al., 2018). Further, a repressed expression level of cGAS or STING was found in a set of late-stage tumor (Song et al., 2017; Xia et al., 2016a, 2016b). Although frequently displaying increased chromosome instability, tumor cells are likely capable of coordinating the cGAS/STING pathway to either suppress or promote malignancy by regulating a distinct array of molecular programs (Bakhoum et al., 2018; Deng et al., 2014). One possibility may involve modulation of the signaling strength of the cGAS/STING pathway in determining the switch between proapoptotic or survival functions under DNA damage (Gulen et al., 2017). Therefore, together with previous reports, our work adds to the knowledge of the roles of the cGAS/STING pathway in diverse cellular or environmental contexts.

Appropriate DNA repair is indispensable to maintain genome stability in response to ionizing radiation-elicited DNA lesions. In this study, our findings illustrate a novel and important role of innate immune machinery in ionizing radiation-regulated deoxyribonucleotide synthesis (Figure 7). Ionizing radiation activates TBK1 in a cGAS/STING-axis-dependent manner, resulting in sequential PRPS1/2 S16 and T228 phosphorylation. This phosphorylation activates PRPS1/2 and boosts deoxyribonucleotide synthesis to support DNA repair and cell proliferation.

Limitations of study

The presented data showed that phosphorylation of PRPS1/2 at T228 markedly enhanced the enzymatic activities of these proteins and overridden the effects of a couple of allosteric regulators, including ADP, IMP, AMP, GMP, or phosphate. Though T228 is located within the catalytic domain, the detailed conformational changes of PRPS1/2 induced by T228 phosphorylation remains unclear. Future work using more advanced approaches are needed to decipher the structural basis of this innate immune response-guided PRPS1/2 activation under ionizing radiation.

STAR★METHODS

Detailed methods are provided in the online version of this paper and include the following:

- KEY RESOURCES TABLE
- RESOURCE AVAILABILITY
  - Lead contact
  - Materials availability
  - Data and code availability
- EXPERIMENTAL MODEL AND SUBJECT DETAILS
  - Mice
  - Cell line culture
- METHOD DETAILS
  - Materials
  - DNA constructs and mutagenesis
  - Cell treatments
  - Cell cycle analysis and synchronization
  - Mass spectrometric analysis
  - BrdU incorporation assay
  - Genomic editing
  - Immunoprecipitation and immunoblot analysis
  - Purification of recombinant proteins
  - Measurement of PRPS activity
  - Quantification of cytosolic DNA
  - *In vitro* ATM kinase assay
  - *In vitro* TBK1 kinase assay
  - RT-PCR analysis
  - Analysis of intermediate metabolites
  - Measurement of intracellular deoxyribonucleotide concentrations
  - Measurement of intracellular R5P levels
  - ADP-binding assay
  - Analyses of NHEJ and HR repair efficiency
  - Analyses of NER repair efficiency
  - Analyses of cellular gap-filling DNA synthesis
  - Liposome-encapsulated deoxyribonucleotide delivery
  - Clonogenic survival assay
  - CCK8 assay
  - Cell survival assays
  - Animal study
  - Diarrhea assessment
  - Immunohistochemical staining
- QUANTIFICATION AND STATISTICAL ANALYSIS

SUPPLEMENTAL INFORMATION

Supplemental information can be found online at https://doi.org/10.1016/j.cmet.2021.07.009.

ACKNOWLEDGMENTS

This work was supported by National Natural Science Foundation of China grants 81672674 (R.L.), 81872218 (R.L.), 81772692 (J.L.), and 82001047 (Y.H.); CAMS Innovation Fund for Medical Sciences (CIFMS) 2019-I2M-5-004 (Q.C.); Scientific Research Program for Young Talents of China National Nuclear Corporation 2020CNNC74 (J.L.); Science & Technology Department of Sichuan Province Applied Basic Research Program 2019YJ0371 (J.L.); Fok Ying Tong Education Foundation grant 161036 (R.L.); Research Funding from West China School/Hospital of Stomatology Sichuan University RCDWJS2020-8 (R.L.); and National Research Foundation of Korea (NRF) grant funded by the Korea Government (MSIT) 2020R1C1C101135 (J.-H.L.).

AUTHOR CONTRIBUTIONS

R.L., J.L., and Q.C. conceived and designed the study; R.L., J.L., J.S., J.-H.L., X.Q., Y.X., Y.H., M.L., and B.Z. performed the experiments; and R.L. wrote the paper with comments from all authors.

DECLARATION OF INTERESTS

The authors declare no competing interests.

Received: March 24, 2020
Revised: April 9, 2021
Accepted: June 12, 2021
Published: August 2, 2021

REFERENCES

Amie, S.M., Noble, E., and Kim, B. (2013). Intracellular nucleotide levels and the control of retroviral infections. Virology *436*, 247–254.

Bakhoum, S.F., Ngo, B., Laughney, A.M., Cavallo, J.A., Murphy, C.J., Ly, P., Shah, P., Sriram, R.K., Watkins, T.B.K., Taunk, N.K., et al. (2018). Chromosomal instability drives metastasis through a cytosolic DNA response. Nature *553*, 467–472.

Blackford, A.N., and Jackson, S.P. (2017). ATM, ATR, and DNA-PK: the trinity at the heart of the DNA damage response. Mol. Cell *66*, 801–817.

Booy, E.P., McRae, E.K., Koul, A., Lin, F., and McKenna, S.A. (2017). The long non-coding RNA BC200 (BCYRN1) is critical for cancer cell survival and proliferation. Mol. Cancer *16*, 109.

Burdette, D.L., Monroe, K.M., Sotelo-Troha, K., Iwig, J.S., Eckert, B., Hyodo, M., Hayakawa, Y., and Vance, R.E. (2011). STING is a direct innate immune sensor of cyclic di-GMP. Nature *478*, 515–518.

Chen, Q., Sun, L., and Chen, Z.J. (2016). Regulation and function of the cGAS-STING pathway of cytosolic DNA sensing. Nat. Immunol. *17*, 1142–1149.

Chen, Y.A., Shen, Y.L., Hsia, H.Y., Tiang, Y.P., Sung, T.L., and Chen, L.Y. (2017). Extrachromosomal telomere repeat DNA is linked to ALT development via cGAS-STING DNA sensing pathway. Nat. Struct. Mol. Biol. *24*, 1124–1131.

Ciccia, A., and Elledge, S.J. (2010). The DNA damage response: making it safe to play with knives. Mol. Cell *40*, 179–204.

Copeland, W.C., Chen, M.S., and Wang, T.S. (1992). Human DNA polymerases alpha and beta are able to incorporate anti-HIV deoxynucleotides into DNA. J. Biol. Chem. *267*, 21459–21464.

Coquel, F., Silva, M.J., Técher, H., Zadorozhny, K., Sharma, S., Nieminuszczy, J., Mettling, C., Dardillac, E., Barthe, A., Schmitz, A.L., et al. (2018). SAMHD1 acts at stalled replication forks to prevent interferon induction. Nature *557*, 57–61.

de Laat, W.L., Jaspers, N.G., and Hoeijmakers, J.H. (1999). Molecular mechanism of nucleotide excision repair. Genes Dev. *13*, 768–785.

Deng, L., Liang, H., Xu, M., Yang, X., Burnette, B., Arina, A., Li, X.D., Mauceri, H., Beckett, M., Darga, T., et al. (2014). STING-dependent cytosolic DNA sensing promotes radiation-induced type I interferon-dependent antitumor immunity in immunogenic tumors. Immunity *41*, 843–852.

Devlin, H.L., Mack, P.C., Burich, R.A., Gumerlock, P.H., Kung, H.J., Mudryj, M., and deVere White, R.W. (2008). Impairment of the DNA repair and growth arrest pathways by p53R2 silencing enhances DNA damage-induced apoptosis in a p53-dependent manner in prostate cancer cells. Mol. Cancer Res. *6*, 808–818.

Dunphy, G., Flannery, S.M., Almine, J.F., Connolly, D.J., Paulus, C., Jønsson, K.L., Jakobsen, M.R., Nevels, M.M., Bowie, A.G., and Unterholzner, L. (2018). Non-canonical activation of the DNA sensing adaptor STING by ATM and IFI16 mediates NF-κB signaling after nuclear DNA damage. Mol. Cell *71*, 745–760.e5.

Ferraro, P., Franzolin, E., Pontarin, G., Reichard, P., and Bianchi, V. (2010). Quantitation of cellular deoxynucleoside triphosphates. Nucleic Acids Res. *38*, e85.

Gao, D., Li, T., Li, X.D., Chen, X., Li, Q.Z., Wight-Carter, M., and Chen, Z.J. (2015). Activation of cyclic GMP-AMP synthase by self-DNA causes autoimmune diseases. Proc. Natl. Acad. Sci. USA *112*, E5699–E5705.

Gibson, R.J., Bowen, J.M., and Keefe, D.M. (2005). Palifermin reduces diarrhea and increases survival following irinotecan treatment in tumor-bearing DA rats. Int. J. Cancer *116*, 464–470.

Gulen, M.F., Koch, U., Haag, S.M., Schuler, F., Apetoh, L., Villunger, A., Radtke, F., and Ablasser, A. (2017). Signalling strength determines proapoptotic functions of STING. Nat. Commun. *8*, 427.

Haag, S.M., Gulen, M.F., Reymond, L., Gibelin, A., Abrami, L., Decout, A., Heymann, M., van der Goot, F.G., Turcatti, G., Behrendt, R., and Ablasser, A. (2018). Targeting STING with covalent small-molecule inhibitors. Nature *559*, 269–273.

Haracska, L., Unk, I., Johnson, R.E., Phillips, B.B., Hurwitz, J., Prakash, L., and Prakash, S. (2002). Stimulation of DNA synthesis activity of human DNA polymerase kappa by PCNA. Mol. Cell. Biol. *22*, 784–791.

Hinz, M., Stilmann, M., Arslan, S.Ç., Khanna, K.K., Dittmar, G., and Scheidereit, C. (2010). A cytoplasmic ATM-TRAF6-cIAP1 module links nuclear DNA damage signaling to ubiquitin-mediated NF-κB activation. Mol. Cell *40*, 63–74.

Hove-Jensen, B. (1988). Mutation in the phosphoribosylpyrophosphate synthetase gene (prs) that results in simultaneous requirements for purine and pyrimidine nucleosides, nicotinamide nucleotide, histidine, and tryptophan in Escherichia coli. J. Bacteriol. *170*, 1148–1152.

Huang, Q., and Shen, H.M. (2009). To die or to live: the dual role of poly(ADP-ribose) polymerase-1 in autophagy and necrosis under oxidative stress and DNA damage. Autophagy *5*, 273–276.

Jensen, K.F., Houlberg, U., and Nygaard, P. (1979). Thin-layer chromatographic methods to isolate 32P-labeled 5-phosphoribosyl-alpha-1-pyrophosphate (PRPP): determination of cellular PRPP pools and assay of PRPP synthetase activity. Anal. Biochem. *98*, 254–263.

Jiang, Y., Qian, X., Shen, J., Wang, Y., Li, X., Liu, R., Xia, Y., Chen, Q., Peng, G., Lin, S.-Y., and Lu, Z. (2015). Local generation of fumarate promotes DNA repair through inhibition of histone H3 demethylation. Nat. Cell Biol. *17*, 1158–1168.

Johnson, R.E., Prakash, S., and Prakash, L. (2000). The human DINB1 gene encodes the DNA polymerase Poltheta. Proc. Natl. Acad. Sci. USA *97*, 3838–3843.

Kornberg, A., Lieberman, I., and Simms, E.S. (1955). Enzymatic synthesis and properties of 5-phosphoribosylpyrophosphate. J. Biol. Chem. *215*, 389–402.

Krishna, T.H., Mahipal, S., Sudhakar, A., Sugimoto, H., Kalluri, R., and Rao, K.S. (2005). Reduced DNA gap repair in aging rat neuronal extracts and its restoration by DNA polymerase beta and DNA-ligase. J. Neurochem. *92*, 818–823.

Lee, J.H., Liu, R., Li, J., Wang, Y., Tan, L., Li, X.J., Qian, X., Zhang, C., Xia, Y., Xu, D., et al. (2018). EGFR-phosphorylated platelet isoform of phosphofructokinase 1 promotes PI3K activation. Mol. Cell *70*, 197–210.e7.

Li, T., and Chen, Z.J. (2018). The cGAS-cGAMP-STING pathway connects DNA damage to inflammation, senescence, and cancer. J. Exp. Med. *215*, 1287–1299.

Li, X., and Heyer, W.D. (2008). Homologous recombination in DNA repair and DNA damage tolerance. Cell Res. *18*, 99–113.

Li, S., Lu, Y., Peng, B., and Ding, J. (2007). Crystal structure of human phosphoribosylpyrophosphate synthetase 1 reveals a novel allosteric site. Biochem. J. *401*, 39–47.

Li, L., Yin, Q., Kuss, P., Maliga, Z., Millán, J.L., Wu, H., and Mitchison, T.J. (2014). Hydrolysis of 2′3′-cGAMP by ENPP1 and design of nonhydrolyzable analogs. Nat. Chem. Biol. *10*, 1043–1048.

Li, X., Jiang, Y., Meisenhelder, J., Yang, W., Hawke, D.H., Zheng, Y., Xia, Y., Aldape, K., He, J., Hunter, T., et al. (2016). Mitochondria-translocated PGK1 functions as a protein kinase to coordinate glycolysis and the TCA cycle in tumorigenesis. Mol. Cell *61*, 705–719.

Lin, R., Elf, S., Shan, C., Kang, H.B., Ji, Q., Zhou, L., Hitosugi, T., Zhang, L., Zhang, S., Seo, J.H., et al. (2015). 6-phosphogluconate dehydrogenase links oxidative PPP, lipogenesis and tumour growth by inhibiting LKB1-AMPK signalling. Nat. Cell Biol. *17*, 1484–1496.

Liu, R., Li, J., Zhang, T., Zou, L., Chen, Y., Wang, K., Lei, Y., Yuan, K., Li, Y., Lan, J., et al. (2014). Itraconazole suppresses the growth of glioblastoma through induction of autophagy: involvement of abnormal cholesterol trafficking. Autophagy *10*, 1241–1255.

Liu, S., Cai, X., Wu, J., Cong, Q., Chen, X., Li, T., Du, F., Ren, J., Wu, Y.T., Grishin, N.V., and Chen, Z.J. (2015). Phosphorylation of innate immune adaptor proteins MAVS, STING, and TRIF induces IRF3 activation. Science *347*, aaa2630.

Liu, H., Zhang, H., Wu, X., Ma, D., Wu, J., Wang, L., Jiang, Y., Fei, Y., Zhu, C., Tan, R., et al. (2018). Nuclear cGAS suppresses DNA repair and promotes tumorigenesis. Nature *563*, 131–136.

Luo, W.W., Li, S., Li, C., Lian, H., Yang, Q., Zhong, B., and Shu, H.B. (2016). iRhom2 is essential for innate immunity to DNA viruses by mediating trafficking and stability of the adaptor STING. Nat. Immunol. *17*, 1057–1066.

Mosbaugh, D.W., and Linn, S. (1984). Gap-filling DNA synthesis by HeLa DNA polymerase alpha in an in vitro base excision DNA repair scheme. J. Biol. Chem. *259*, 10247–10251.

Nosal, J.M., Switzer, R.L., and Becker, M.A. (1993). Overexpression, purification, and characterization of recombinant human 5-phosphoribosyl-1-pyrophosphate synthetase isozymes I and II. J. Biol. Chem. *268*, 10168–10175.

Peng, G., Yim, E.K., Dai, H., Jackson, A.P., Burgt, I.V., Pan, M.R., Hu, R., Li, K., and Lin, S.Y. (2009). BRIT1/MCPH1 links chromatin remodelling to DNA damage response. Nat. Cell Biol. *11*, 865–872.

Pierce, A.J., Johnson, R.D., Thompson, L.H., and Jasin, M. (1999). XRCC3 promotes homology-directed repair of DNA damage in mammalian cells. Genes Dev. *13*, 2633–2638.

Pilli, M., Arko-Mensah, J., Ponpuak, M., Roberts, E., Master, S., Mandell, M.A., Dupont, N., Ornatowski, W., Jiang, S., Bradfute, S.B., et al. (2012). TBK-1 promotes autophagy-mediated antimicrobial defense by controlling autophagosome maturation. Immunity *37*, 223–234.

Qu, J., Sun, W., Zhong, J., Lv, H., Zhu, M., Xu, J., Jin, N., Xie, Z., Tan, M., Lin, S.-H., et al. (2017). Phosphoglycerate mutase 1 regulates dNTP pool and promotes homologous recombination repair in cancer cells. J. Cell Biol. *216*, 409–424.

Schrempf, A., Slyskova, J., and Loizou, J.I. (2021). Targeting the DNA repair enzyme polymerase θ in cancer therapy. Trends Cancer *7*, 98–111.

Shen, J.C., Fox, E.J., Ahn, E.H., and Loeb, L.A. (2014). A rapid assay for measuring nucleotide excision repair by oligonucleotide retrieval. Sci. Rep. *4*, 4894.

Shu, C., Yi, G., Watts, T., Kao, C.C., and Li, P. (2012). Structure of STING bound to cyclic di-GMP reveals the mechanism of cyclic dinucleotide recognition by the immune system. Nat. Struct. Mol. Biol. *19*, 722–724.

So, S., Davis, A.J., and Chen, D.J. (2009). Autophosphorylation at serine 1981 stabilizes ATM at DNA damage sites. J. Cell Biol. *187*, 977–990.

Song, S., Peng, P., Tang, Z., Zhao, J., Wu, W., Li, H., Shao, M., Li, L., Yang, C., Duan, F., et al. (2017). Decreased expression of STING predicts poor prognosis in patients with gastric cancer. Sci. Rep. *7*, 39858.

Spyrou, G., and Reichard, P. (1988). Dynamics of the thymidine triphosphate pool during the cell cycle of synchronized 3T3 mouse fibroblasts. Mutat. Res. *200*, 37–43.

Stettler, M., Jaccard, N., Hacker, D., De Jesus, M., Wurm, F.M., and Jordan, M. (2006). New disposable tubes for rapid and precise biomass assessment for suspension cultures of mammalian cells. Biotechnol. Bioeng. *95*, 1228–1233.

Taniguchi, T., Garcia-Higuera, I., Xu, B., Andreassen, P.R., Gregory, R.C., Kim, S.T., Lane, W.S., Kastan, M.B., and D'Andrea, A.D. (2002). Convergence of the fanconi anemia and ataxia telangiectasia signaling pathways. Cell *109*, 459–472.

Turenne, G.A., Paul, P., Laflair, L., and Price, B.D. (2001). Activation of p53 transcriptional activity requires ATM's kinase domain and multiple N-terminal serine residues of p53. Oncogene *20*, 5100–5110.

Vanpouille-Box, C., Alard, A., Aryankalayil, M.J., Sarfraz, Y., Diamond, J.M., Schneider, R.J., Inghirami, G., Coleman, C.N., Formenti, S.C., and Demaria, S. (2017). DNA exonuclease Trex1 regulates radiotherapy-induced tumour immunogenicity. Nat. Commun. *8*, 15618.

Vincent, F., Ceraline, J., Goldblum, S., Klein-Soyer, C., and Bergerat, J.P. (2001). A new flow cytometric method to follow DNA gap filling during nucleotide excision repair of UVc-induced damage. Cytometry *45*, 96–101.

Wang, Q., Liu, X., Cui, Y., Tang, Y., Chen, W., Li, S., Yu, H., Pan, Y., and Wang, C. (2014). The E3 ubiquitin ligase AMFR and INSIG1 bridge the activation of TBK1 kinase by modifying the adaptor STING. Immunity *41*, 919–933.

Wellinger, R.E., and Thoma, F. (1996). Taq DNA polymerase blockage at pyrimidine dimers. Nucleic Acids Res. *24*, 1578–1579.

Weterings, E., and Chen, D.J. (2008). The endless tale of non-homologous end-joining. Cell Res. *18*, 114–124.

Wolf, C., Rapp, A., Berndt, N., Staroske, W., Schuster, M., Dobrick-Mattheuer, M., Kretschmer, S., König, N., Kurth, T., Wieczorek, D., et al. (2016). RPA and Rad51 constitute a cell intrinsic mechanism to protect the cytosol from self DNA. Nat. Commun. *7*, 11752.

Xia, T., Konno, H., Ahn, J., and Barber, G.N. (2016a). Deregulation of STING signaling in colorectal carcinoma constrains DNA damage responses and correlates with tumorigenesis. Cell Rep. *14*, 282–297.

Xia, T., Konno, H., and Barber, G.N. (2016b). Recurrent loss of STING signaling in melanoma correlates with susceptibility to viral oncolysis. Cancer Res. *76*, 6747–6759.

Xu, X., Tsvetkov, L.M., and Stern, D.F. (2002). Chk2 activation and phosphorylation-dependent oligomerization. Mol. Cell. Biol. *22*, 4419–4432.

You, Z., Bailis, J.M., Johnson, S.A., Dilworth, S.M., and Hunter, T. (2007). Rapid activation of ATM on DNA flanking double-strand breaks. Nat. Cell Biol. *9*, 1311–1318.

Zhou, Y., Tozzi, F., Chen, J., Fan, F., Xia, L., Wang, J., Gao, G., Zhang, A., Xia, X., Brasher, H., et al. (2012). Intracellular ATP levels are a pivotal determinant of chemoresistance in colon cancer cells. Cancer Res. *72*, 304–314.

STAR★METHODS

KEY RESOURCES TABLE

REAGENT or RESOURCE	SOURCE	IDENTIFIER
Antibodies		
Rabbit polyclonal antibody anti-PRPS1/2 pS16	Boer Biotechnology	N/A
Rabbit polyclonal antibody anti-PRPS1/2 pT228	Boer Biotechnology	N/A
Rabbit polyclonal antibody anti-PRPS1	Boer Biotechnology	N/A
Rabbit polyclonal antibody anti-PRPS2	Boer Biotechnology	N/A
Rabbit monoclonal antibody anti-TBK1 pS172	Cell Signaling Technology	Cat# 5483; RRID: AB_10693472
Rabbit monoclonal anti-STING	Cell Signaling Technology	Cat# 13647; RRID: AB_2732796
Rabbit monoclonal antibody anti-STING pS366	Cell Signaling Technology	Cat# 50907; RRID: AB_2827656
Rabbit monoclonal antibody anti-IRF3 pS396	Cell Signaling Technology	Cat# 29047; RRID: AB_2773013
Rabbit monoclonal antibody anti-H2AX	Cell Signaling Technology	Cat# 7631; RRID: AB_10860771
Mouse monoclonal antibody anti-γH2AX	Cell Signaling Technology	Cat# 80312; RRID: AB_2799949
Rabbit monoclonal antibody anti-IKKε	Cell Signaling Technology	Cat# 3416; RRID: AB_1264180
Rabbit polyclonal antibody anti-NIK	Cell Signaling Technology	Cat# 4994; RRID: AB_2297422
Mouse monoclonal antibody anti-PRPS1/2	Santa Cruz Biotechnology	Cat# sc-100822; RRID: AB_2268859
Rabbit polyclonal antibody anti-Tubulin	Cell Signaling Technology	Cat# 2144; RRID: AB_2210548
Rabbit polyclonal antibody anti-Ki67	EMD Millipore	Cat# AB9260; RRID: AB_2142366
Mouse monoclonal antibody anti-GST	Santa Cruz Biotechnology	Cat# sc-138; RRID: AB_627677
Mouse monoclonal antibody anti-Flag	Sigma	Cat#F3165; RRID: AB_259529
Rabbit monoclonal antibody anti-His	Cell Signaling Technology	Cat# 12698; RRID: AB_2744546
Rabbit monoclonal antibody anti-HA	Cell Signaling Technology	Cat# 3724; RRID: AB_1549585
Rabbit polyclonal antibody anti-human ATM pS1981/ mouse ATM pS1987	R&D systems	Cat# AF1655
Rabbit monoclonal antibody anti-ATM	ABCAM	Cat# ab201022
Rabbit monoclonal antibody anti-TBK1	ABCAM	Cat# ab40676; RRID: AB_776632
Rabbit monoclonal antibody anti-TREX1	ABCAM	Cat# ab185228; RRID: AB_2885196
Rabbit polyclonal antibody anti-ENPP1	Cell Signaling Technology	Cat# 2070; RRID: AB_2270873
Bacterial and virus strains		
BL21(DE3)	EMD Millipore	Cat#71401-3
Chemicals, peptides, and recombinant proteins		
ATP	Sigma-Aldrich	Cat# A7699; CAS: 34369-07-8
ANTI-FLAG M2 agarose affinity gel	Sigma-Aldrich	Cat# A2220
Flag peptide	Sigma-Aldrich	Cat# F4799
[γ-^{32}P]-ATP	MP Biomedicals	Cat# 0135001
Hoechst 33258	Sigma-Aldrich	Cat# 94403; CAS: 23491-45-4
KU55933	Sigma-Aldrich	Cat# SML1109; CAS: 587871-26-9
Lovastatin	Sigma-Aldrich	Cat# PHR1285; CAS: 75330-75-5
ADP	Sigma-Aldrich	Cat# C7344; CAS: 119340-53-3
MMS	Sigma-Aldrich	Cat# 129925; CAS: 66-27-3
cGAMP	InvivoGen	Cat# tlrl-nacga23; CAS: 1441190-66-4
C-di-GMP	InvivoGen	Cat# tlrl-nacdg; CAS: 61093-23-0
BX795	InvivoGen	Cat# tlrl-bx7; CAS: 702675-74-9

(*Continued on next page*)

Continued

REAGENT or RESOURCE	SOURCE	IDENTIFIER
H-151	MedChemExpress	Cat# HY-112693; CAS: 941987-60-6
C-170	MedChemExpress	Cat# HY-138682; CAS: 346691-38-1
NU7441	MedChemExpress	Cat# HY-11006; CAS: 503468-95-9
[13C6]-glucose	Cambridge Isotope Laboratories	Cat# CLM-1396-10; CAS: 110187-42-3
[13C2,15N]-glycine	Cambridge Isotope Laboratories	Cat# CNLM-1673-H-MPT; CAS: 211057-02-2
[13C5,15N4]-hypoxanthine	Cambridge Isotope Laboratories	Cat# CNLM-7894-PK; CAS: 1987883-25-9
Critical commercial assays		
Colorimetric Cell Proliferation ELISA kit	Sigma	Cat# 11647229001
Nuclei/cytosol fractionation kit	BioVision	Cat# K266
Cell Counting Kit 8	ABCAM	Cat# ab228554
Phosphate Colorimetric Assay Kit	BioVision	Cat# K410
Vectastain Elite ABC kit	Vector Laboratories	Cat# PK-6100
Experimental models: cell lines		
Human: FHs 74 Int cells	ATCC	Cat# CCL-241
Human: HUVEC cells	ATCC	Cat# CRL-1730
Human: SK-MEL-5 cells	ATCC	Cat# HTB-70
Human: Saos-2 cells	ATCC	Cat# HTB-85
Human: HOK cells	ScienCell	Cat# 2610
Experimental models: organisms/strains		
Mouse: C57BL/6	CHENGDU DOSSY EXPERIMENTAL ANIMALS	N/A
Oligonucleotides		
Targeting sequence for control shRNA, GCT TCT AAC ACC GGA GGT CTT	This paper	N/A
Targeting sequence for PRPS1 shRNA, GAT AAT ATG ATC TGC ACC T	This paper	N/A
Targeting sequence for PRPS2 shRNA, TAA ACC AAT ACA AGC ACT G	This paper	N/A
Targeting sequence for cGAS shRNA, AAA TTT CAC AAA GTA ATA T	This paper	N/A
Targeting sequence for STING shRNA, TCC ATT CCA CTG ATG AGG A	This paper	N/A
Targeting sequence for TBK1 shRNA, AAA GGC ATT CAT TTA ATG C	This paper	N/A
Recombinant DNA		
Plasmid: pCold I-PRPS1	This paper	N/A
Plasmid: pCold I-PRPS1 S16A	This paper	N/A
Plasmid: pCold I-PRPS2	This paper	N/A
Plasmid: pCold I-PRPS2 S16A	This paper	N/A
Plasmid: pCold I-PRPS1 T228A	This paper	N/A
Plasmid: pCold I-PRPS2 T228A	This paper	N/A
Plasmid: pGEX-4T-1-TBK1	This paper	N/A
Plasmid: pGEX-4T-1-TBK1 S172E	This paper	N/A
Plasmid: pGEX-4T-1-ENPP1	This paper	N/A
Plasmid: pcDNA 3.1-Flag-PRPS1	This paper	N/A
Plasmid: pcDNA 3.1-Flag-PRPS2	This paper	N/A
Plasmid: pcDNA 3.1-Flag-PRPS1 T228A	This paper	N/A
Plasmid: pcDNA 3.1-His-PRPS2	This paper	N/A
Plasmid: pcDNA 3.1-His-PRPS2 T228A	This paper	N/A

(*Continued on next page*)

Continued

REAGENT or RESOURCE	SOURCE	IDENTIFIER
Plasmid: pcDNA 3.1-Flag-TBK1	This paper	N/A
Plasmid: pcDNA 3.1-Flag-ATM	This paper	N/A
Plasmid: pcDNA 3.1-Flag-ATM KD	This paper	N/A
Plasmid: pcDNA 3.1-His-PRPS2 S16A	This paper	N/A
Plasmid: pcDNA 3.1-HA-PRPS1	This paper	N/A
Plasmid: pcDNA 3.1-HA-PRPS1 S16A	This paper	N/A
Plasmid: pcDNA 3.1-Flag-cGAS	This paper	N/A
Plasmid: pcDNA 3.1-Flag-cGAS Y215E	This paper	N/A
Plasmid: pcDNA 3.1-HA-STING	This paper	N/A
Plasmid: pcDNA 3.1-HA-STING E260A	This paper	N/A
Plasmid: pcDNA 3.1-HA-STING S366A	This paper	N/A
Plasmid: pEGFP-TREX1	This paper	N/A
Plasmid: PX458	Addgene	Plasmid #48138

RESOURCE AVAILABILITY

Lead contact

Further information and requests for resources and reagents should be directed to and will be fulfilled by the lead contact, Rui Liu (liurui_scu@hotmail.com).

Materials availability

All stable and unique reagents generated in this study are available from the Lead Contact subject to a Materials Transfer Agreement.

Data and code availability

- All data reported in this paper will be shared by the lead contact upon request.
- This paper does not report original code.
- Any additional information required to reanalyze the data reported in this paper is available from the lead contact upon request.

EXPERIMENTAL MODEL AND SUBJECT DETAILS

Mice

Male C57BL/6 mice, aged 6-8 weeks and weighing 18-22 g, were obtained from Dossy experimental animals (Chengdu, China) and used for whole body or abdominal irradiation.

Cell line culture

FHs 74 Int, HUVEC, SK-MEL-5 and Saos-2 cells were obtained from ATCC. FHs 74 Int cells were maintained with HybriCare medium ATCC 46X supplemented with 30 ng/ml epidermal growth factor (EGF) and 10% fetal bovine serum. HUVEC cells were cultured with F-12K medium supplemented with 10% fetal bovine serum. SK-MEL-5 and Saos-2 cells were cultured with Dulbecco's Modified Eagle Medium supplemented with 10% fetal bovine serum. HOK cells were obtained from ScienCell (Carlsbad, CA), and were maintained in Oral Keratinocyte Medium (Carlsbad, CA) supplemented with 10% fetal bovine serum.

METHOD DETAILS

Materials

Rabbit polyclonal antibodies recognizing unmodified PRPS1, PRPS2 phosphorylated PRPS1/2 pS16 and phosphorylated PRPS1/2 pT228 were customized from Boer Biotechnology (Chengdu, China). To prepare the PRPS1 antibody, a synthetic peptide (KWIRENISEWRNCT) was injected into rabbits. Rabbit serum was collected and purified using an affinity column conjugated with recombinant PRPS2 protein to exclude antibodies recognizing PRPS2, followed by an affinity column conjugated with recombinant PRPS1 protein to bind to and purify the antibody. The PRPS2 antibody was generated by using a peptide immunogen (QWIRENIAEWKNCI). To prepare the PRPS1/2 pS16 or PRPS1/2 pT228 antibodies, peptides containing PRPS1/2 pS16 or pT228 was injected into rabbits. The rabbit serum was collected and purified using an affinity column conjugated with non-modified peptide to exclude antibodies recognizing non-phosphorylated PRPS1/2, followed by an affinity column conjugated with PRPS1/2 pS16 or pT228 peptide to bind to and purify the antibody.

Antibodies recognizing TBK1 pS172, STING, STING pS366, IRF3 pS396, H2AX, His, HA, γH2AX, IKKε, Tubulin and NIK were obtained from Cell Signaling Technology. The antibody recognizing both PRPS1 and PRPS2, GST was obtained from Santa Cruz. Antibodies recognizing TBK1, ATM, TREX1 and were obtained from Abcam. Antibody recognizing human ATM pS1981 and mouse ATM pS1987 were purchased from R&D systems. Antibody recognizing Ki67 was purchased from EMD Millipore. Antibody recognizing Flag, anti-Flag M2 agarose beads, streptavidin-conjugated agarose beads, Hoechst 33258, ATP, KU55933, Lovastatin, ADP, MMS, and bovine serum albumin were purchased from Sigma. cGAMP, C-di-GMP, and BX795 were obtained from InvivoGen. NU7441, H-151 and C-170 were obtained from MedChemExpress. Horseradish peroxidase-conjugated goat anti-mouse or rabbit secondary antibodies were obtained from Thermo Fisher Scientific. [γ-^{32}P]-ATP was purchased from MP Biomedicals. [$^{13}C_6$]-glucose, [$^{13}C_2$,^{15}N]-glycine, and [$^{13}C_5$,$^{15}N_4$]-hypoxanthine were purchased from Cambridge Isotope Laboratories.

DNA constructs and mutagenesis

PCR-amplified human PRPS1, PRPS2, ATM, TBK1, STING and ENPP1 were subcloned into pcDNA3.1/hygro(+)-Flag, pcDNA3.1/hygro(+)-HA, pCDH-SFB, or pCold I (His) vectors. Mutants were constructed using the QuikChange site-directed mutagenesis kit (Stratagene, La Jolla, CA).

The following pGIPZ shRNAs were used: control shRNA, GCT TCT AAC ACC GGA GGT CTT; PRPS1 shRNA, GAT AAT ATG ATC TGC ACC T; PRPS2 shRNA, TAA ACC AAT ACA AGC ACT G (targeting non-coding region); cGAS shRNA, AAA TTT CAC AAA GTA ATA T; STING shRNA, TCC ATT CCA CTG ATG AGG A (targeting non-coding region); TBK1 shRNA, AAA GGC ATT CAT TTA ATG C (targeting non-coding region). ShRNAs targeting cGAS, IKKε or NIK were purchased from OriGene Technologies (Rockville, MD).

ShRNA-resistant PRPS1 vector was generated by introducing nonsense mutations of A568C, T571C, T574C and T577C. ShRNA-resistant cGAS vector was generated by introducing nonsense mutations of C747T, T750C, G753C and A756G.

Cell treatments

Ionizing radiation was performed using a Cr^{137} γ-ray irradiator (Atomic Energy of Canada, Chalk River, Ontario, Canada) at 2 Gy/min at room temperature. UVC irradiation (254 nm) was performed at a rate of 0.5 J/m^2/s to achieve the cumulative desired doses, which was measured by a UV radiometer (Tokyo Kogaku Kikai, Tokyo, Japan). The culture dishes were replenished with fresh culture medium immediately after irradiation.

To generate stable shRNA-depleted cells, cells were transfected with shRNA plasmids and selected by puromycin. To stable generate gene-expressing cells, shRNA-depleted cells were infected with lentivirus carrying WT or mutant gene and selected by hygromycin.

Transfection of plasmids was performed by using Lipofectamine 2000. Transfection of cGAMP or C-di-GMP was performed by using Lipofectamine RNAiMax.

Delivery of recombinant protein was performed by using Lipodin-Pro-Protein Transfection Reagent (ABBIOTEC), following the manufacturer's instructions. Briefly, 20 μl of protein solution (diluted in PBS, 100 μg/ml) was mixed with 4 μl of Lipodin-Pro reagent, and the mixture was incubated at room temperature for 15 min. After 100 μl of serum-free medium was added, the mixture was transferred immediately into one well of a 12-well plate containing 2 × 10^5 cells.

Cell cycle analysis and synchronization

Cells were fixed with 70% ethanol on ice for at least 30 min, washed twice with ice-cold PBS and resuspended in 100 μg/ml RNase A (Invitrogen, Paisley, UK) in PBS. After incubation on ice for 30 min, the cells were stained with propidium iodide (BD Biosciences, Franklin Lakes, NJ) at 25 °C in the dark for 30 min. Thereafter, the DNA contents of the stained cells were analyzed by a flow cytometer (BD Accuri C6, BD Biosciences). The data were finally presented as percentages of the cells in G1, S, and G2/M phases using FlowJo 10.4 software (Verity Software House, Topsham, ME).

Cell synchronization was performed according to previous report (Booy et al., 2017). Cells (30-40% in confluence) were washed twice with phosphate-buffered saline (PBS), treated with 20 μM lovastatin for 24 h. Cells were washed twice with PBS and released in fresh media containing 1 mM mevalonate.

Mass spectrometric analysis

Protein bands visualized via Coomassie Brilliant Blue staining were excised from SDS-PAGE gels and digested in 50 mM ammonium bicarbonate buffer containing RapiGest (Waters Corporation) overnight at 37°C with 200 ng of modified sequencing-grade trypsin (Promega). The digested samples were analyzed using high-sensitivity liquid chromatography tandem mass spectrometry with an Orbitrap Elite mass spectrometer (Thermo Fisher Scientific). Proteins were identified by searching the fragment spectra against the Swiss-Prot protein database (EBI) using the Mascot search engine (version 2.3; Matrix Science) with the Proteome Discoverer software program (version 1.4; Thermo Fisher Scientific).

BrdU incorporation assay

Cell proliferation was measured by BrdU incorporation assay using a colorimetric Cell Proliferation ELISA kit (Sigma) following manufacturer's instructions. 48 h after the indicated irradiation, cells in 96-well plates were incubated with 10 mM BrdU for 12 h, and BrdU signal was measured by a multi-detection microplate reader (BMG Labtech).

Genomic editing

Genomic mutations in FHs 74 Int cells were created using the CRISPR/Cas9 system as described previously (Li et al., 2016). Single guide RNAs (sgRNAs) were designed to target the genomic areas adjacent to human PRPS1 or PRPS2 mutation sites. Annealed guide oligos containing overhangs were inserted into the high-fidelity PX458-HF vector (Addgene) digested with the BbsI restriction enzyme. In a 24-well plate, FHs 74 Int cells at 60% confluence were co-transfected with a single-stranded donor oligonucleotide (20 pmoles) used as a template to introduce the mutations, a vector (0.5 μg) able to co-express an sgRNA targeting the PRPS1 or PRPS2 gene, and WT hSpCas9 tagged with green fluorescent protein. 24 hours after transfection, cells were trypsinized and diluted in medium for single-cell seeding into a 96-well plate, and green fluorescent protein-positive cells were marked and subjected to genomic DNA extraction. Genotyping was performed by sequencing PCR products amplified from primers spanning the mutation area.

Immunoprecipitation and immunoblot analysis

Extraction of proteins from cultured cells was performed with lysis buffer (50 mM Tris-HCl [pH 7.5], 0.1% SDS, 1% Triton X-100, 150 mM NaCl, 1 mM dithiothreitol, 0.5 mM EDTA, 100 μM PMSF, 100 μM leupeptin, 1 μM aprotinin, 100 μM sodium orthovanadate, 100 μM sodium pyrophosphate, and 1 mM sodium fluoride). Cell extracts were clarified by centrifugation at 13,400 g, and the supernatants (2 mg protein/ml) were subjected to immunoprecipitation with the indicated antibodies. After overnight incubation at 4°C, protein A or G agarose beads were added and left for an additional 3 h. Immunocomplexes were washed with lysis buffer 3 times and then subjected to immunoblot analyses with corresponding antibodies as described previously (Liu et al., 2014). The band intensity was quantified using Image J software.

Purification of recombinant proteins

Expression of Flag-PRPS1, His-PRPS1, His-PRPS2, GST-TBK1 and mutants was induced in bacteria, and these proteins were purified as described previously (Li et al., 2016). Briefly, BL21(DE3) cells expressing His-, or GST-tagged proteins were cultured in 250 ml of LB medium and treated with isopropyl β-D-1-thiogalactopyranoside (IPTG) for 16 h at 30 °C before lysis via sonication.

Flag-tagged ATM and GST-tagged extracellular region of ENPP1 (aa 98-925) proteins were expressed in 293T cells. Briefly, a pcDNA3.1 plasmid (10 μg) expressing Flag-ATM or GST-ENPP1 was transfected into 293T cells seeded in a 15 cm-diameter dish with 70% confluence. 48 hours after transfection, the cells were incubated with fresh DMEM supplemented with 10% bovine calf serum for 1 h and then harvested with a non-denaturing lysis buffer (20 mM Tris HCl pH 8.0, 137 mM NaCl, 1% NP-40).

For purification of His-tagged proteins, cell lysates were loaded onto a Ni-NTA column (GE Healthcare Life Sciences) followed by washing with five column volumes of 20 mM imidazole and subsequent elution with 250 mM imidazole.

For purification of Flag-tagged proteins, cell lysates were loaded onto a column containing anti-Flag M2 agarose affinity gel, followed by washing with five column volumes of phosphate-buffered saline (PBS) and subsequent elution with 100 μg/ml Flag peptide. The proteins in 10-kDa spin columns were desalted by washing twice with ice-cold PBS.

For GST-tagged proteins, cell lysates were loaded onto a GSTrap HP column (GE Healthcare Life Sciences) followed by washing with five column volumes of PBS and subsequent elution with 10 mM reduced glutathione.

The proteins were then loaded onto a HiPrep 16/60 Sephacryl S-200 HR gel filtration column (GE Healthcare Life Sciences) to remove contaminated proteins. The purification efficiency was examined using SDS-PAGE and colloidal Coomassie Brilliant Blue (G-250) staining, with superior sensitivity (as low as 1 ng of protein per band).

Measurement of PRPS activity

To measure the activity of purified or immunoprecipitated PRPS protein, PRPS protein (10 ng) was incubated in 100 μl of reaction buffer (50 mmol/l Tris-HCl [pH 7.5], 0.4 mmol/l NADH, 1.8 mmol/l phosphoenolpyruvate, 6 mmol/L $MgCl_2$, 31 mmol/l $NaHCO_3$, 7 U pyruvate kinase, 10 U lactic dehydrogenase, and 10 U myokinase). The reaction was initiated by adding 4.7 mmol/L R5P and 3.2 mmol/l ATP at 25°C into the system. A series of reactions were performed:

a. PRPS1/2 catalyzes: ATP and R5P → PRPP and AMP;
b. Myokinase catalyzes: ATP and AMP → ADP;
c. Pyruvate kinase catalyzes: phosphoenolpyruvate and ADP → pyruvate and ATP;
d. Lactic dehydrogenase catalyzes: pyruvate and NADH → lactate and NAD.

The absorbance value of the reaction system was measured at 340 nm (NADH) in kinetic mode for 5 minutes using a multi-detection microplate reader (BMG Labtech). Myokinase, pyruvate kinase, lactic dehydrogenase and phosphoenolpyruvate were excessive in the system to ensure complete consumption of AMP generated by the PRPS protein. The amount of PRPS protein in the immunoprecipitates or eluates was quantified by immunoblot using purified His-PRPS protein as standard.

To measure the endogenous PRPS activity in the cell lysates, we performed the assay using [γ-^{32}P]ATP, followed by separation of PRPP by a reported thin-layer chromatographic method (Jensen et al., 1979), and the radioactive PRPS was quantified by liquid scintillation counting. Briefly, 1×10^7 cells were quickly washed and homogenized in 1 ml reaction buffer on ice. 100 μl of cell lysates was supplemented with 4.7 mmol/l R5P, 3.2 mmol/l ATP and 20 μCi [γ-^{32}P]ATP and incubated at 25°C for 30 min. 10 μl reaction sample

was mixed with 5 μl 0.33 M formic acid, and applied to PEI sheets. The sheets were chromatographed in 0.85 M potassium phosphate at pH 3.4. The radioactivity in the PRPP spots was determined by liquid scintillation counting, and normalized to the amount of PRPS protein.

Quantification of cytosolic DNA

The mitochondria-free cytosolic fraction was prepared using a Mitochondria/Cytosol Fractionation Kit (BioVision). A total of 5 x 10^7 cells were washed with PBS, and resuspended in Cytosol Extraction Buffer Mix containing DTT and protease inhibitors. Cells were homogenized, centrifuged at 700 g at 4 °C for 10 min, and then centrifuged at 10000 g at 4 °C for 30 min. The supernatant was collected as the cytosolic fraction without mitochondria. Cytosolic DNA was quantified using the SpectraMax Quant AccuClear Nano dsDNA Assay kit (Molecular Devices, Part # R8357) (Vanpouille-Box et al., 2017). The samples were read using the FlexStation 3 multi-mode microplate reader.

In vitro ATM kinase assay

The *in vitro* ATM kinase assay was performed as described earlier (Peng et al., 2009). Briefly, 10 ng purified ATM protein and 100 ng purified PRPS1 or PRPS2 proteins were resuspended in 50 μl of kinase buffer containing 0.5 mM ATP, 1 mM sodium fluoride, 1 mM Na_3VO_4, and 20 mM glycerophosphate in the presence or absence of 10 μCi [γ-^{32}P]ATP. The kinase reaction was performed at 30 °C for 20 min and stopped by the addition of SDS sample buffer. The protein samples were resolved by SDS-PAGE, and were detected by immunoblotting with the indicated antibodies or by autoradiography.

In vitro TBK1 kinase assay

The purified WT TBK1 or TBK1 S172E mutant protein (20 ng) was incubated with 100 ng purified PRPS1 or PRPS2 proteins in kinase buffer (0.5 mM ATP, 25 mM Tris-HCl (pH 7.5), 5 mM β-glycerophosphate, 2 mM dithiothreitol, 0.1 mM Na_3VO_4 and 10 mM $MgCl_2$) in the presence or absence of 10 μCi [γ-^{32}P]ATP for 30 min at 30 °C. The reaction was stopped by the addition of SDS sample buffer. The protein samples were resolved by SDS-PAGE, and detected by immunoblotting with the indicated antibodies or by autoradiography.

RT-PCR analysis

Total RNA was extracted with TRIzol (Thermo Fisher Scientific) and reverse transcribed with Maxima H Minus Reverse Transcriptase (Thermo Fisher Scientific). Real-time PCR was performed with AccuPower 2× Greenstar qPCR Master Mix (Bioneer) on a 7900HT Fast Real-Time PCR System (Applied Biosystems). Data were normalized to ACTB. The primers used were as follows: IFNB, forward, 5′-AAA CTC ATG AGC AGT CTG CA-3′; reverse, 5′-AGG AGA TCT TCA GTT TCG GAG G-3′; human ACTB, forward, 5′-GGC ATC CTC ACC CTG AAG TA-3′; reverse, 5′-AG AGG CGT ACA GGG ATA GCA-3′.

Analysis of intermediate metabolites

Metabolites were analyzed by high resolution mass spectrometry (HRMS). For cell samples, 5×10^7 cells were quickly washed with ice-cold PBS to remove extra medium components. Deoxyribonucleotides and metabolites were extracted using 90/9/1 (v/v/v) acetonitrile/water/formic acid, and PRPP were extracted by 75/25 (v/v) ethanol/10 mmol/l HEPES buffer. The samples were centrifuged at 17,000 g for 5 minutes at 4°C, and supernatants were transferred to clean tubes, followed by evaporation to dryness using nitrogen. Samples were reconstituted in 0.2% ammonium hydroxide in ammonium acetate (10 mmol/l), and then 10 μl was injected into a Thermo Scientific Vanquish liquid chromatography system containing a Thermo Hypercarb 100 × 3 mm 3 μm HPLC column heated to 35°C with mobile phase A (MPA) consisting of 0.2% ammonium hydroxide in ammonium acetate (10 mmol/L) and mobile phase B (MPB) consisting of 0.2% ammonium hydroxide in acetonitrile. At a flow rate of 0.3 mL/minute, the gradient elution program was: 0 minute (0% MPB)-2.0 minutes (0% MPB)-15.0 minutes (30% MPB)-15.1 minutes (95% MPB)-20.0 minutes (95% MPB)-20.1 minutes (0% MPB)-25.0 minutes (STOP). Data were acquired using a Thermo Orbitrap Fusion Tribrid Mass Spectrometer via Selected Ion Mode (SIM) electrospray positive mode. Peak integration and area calculation were performed by using Thermo TraceFinder software.

For measurement of cGAMP, the samples were analyzed on a Shimadzu HPLC with an autosampler set at 4 °C and connected to an AB Sciex 4000 QTRAP. 10 μl sample was injected onto a Biobasic AX LC column (5 μm, 50×3 mm; Thermo Scientific). The mobile phase consisted of 100 mM ammonium carbonate (A) and 0.1% formic acid in acetonitrile (B). The initial condition was 90% B, which was maintained for 0.5 min. The mobile phase was ramped to 30% A from 0.5 min to 2.0 min, maintained at 30% A from 2.0 min to 3.5 min, ramped to 90% B from 3.5 min to 3.6 min and maintained at 90% B from 3.6 min to 5 min. The flow rate was set to 0.6 ml/min. The mass spectrometer was operated in electrospray positive-ion mode with the source temperature set at 500 °C. Declustering and collision-induced dissociation were achieved with nitrogen gas. For each molecule, the MRM transition(s) (m/z), DP (V) and CE (V) were as follows: cGAMP (675>136, 121, 97; 675>312, 121, 59; 675>152, 121, 73), and the internal standard cyclic GMP-[$^{13}C_{10}$,$^{15}N_5$]AMP (690>146, 111, 101; 690>152, 111, 45; 690>327, 111, 47)

For tracing metabolic flux, cells were washed immediately after exposure to ionizing radiation, and then incubated with [$^{13}C_6$]-glucose (10 mmol/l), [$^{13}C_2$,^{15}N]-glycine (0.4 mmol/l) or [$^{13}C_5$,$^{15}N_4$]-hypoxanthine (0.1 mmol/l) for the indicated times. The metabolites were analyzed by HRMS with a similar protocol.

Intracellular phosphate was measured by using Phosphate Colorimetric Assay Kit (BioVision), according to manufacturer's instructions.

Measurement of intracellular deoxyribonucleotide concentrations

After the indicated treatment, 1×10^8 cells were harvested using trypsin, washed twice with PBS, and suspended in 1 ml PBS. A total of 900 μl of the cell suspension was used to measure the content of deoxyribonucleotides with the aforementioned method. The cell volume was determined according to previous report (Stettler et al., 2006). Briefly, the resting 100 μl cell suspension was transferred to a mini PCV tube (Techno Plastics Products AG, Trasadingen, Switzerland), and centrifuged at 2500 g for 2 min. The volume of the cell pellet was measured according to the capillary graduation on the PCV tube. The intracellular concentration of deoxyribonucleotides was calculated as follows:

$$\text{intracellular concentration} = \frac{\text{content of deoxyribonucleotides in cells from 900 μl cell suspension}}{9\times \text{ volume of cells from 100 μl cell suspension}}$$

Data in Table S1 represent the mean ± SD from three independent experiments.

Measurement of intracellular R5P levels

The intracellular concentration of R5P was measured using previously described methods, with some modifications (Lin et al., 2015). In brief, 1×10^6 cells were washed, homogenized, centrifuged at 15000 g for 10 min, and the supernatants were deproteinized using 10 kDa spin columns (EMD Millipore). The flow-through was mixed with 2 × reaction buffer (100 mmol/l Tris-HCl [pH 8.0], 3.4 mmol/l ribulose-5-P, 0.004% w/v thiamine pyrophosphate, 30 mmol/l $MgCl_2$, 0.4 mmol/L NADH, 1 U α-glycerophosphate dehydrogenase, 10 U triosephosphate isomerase, and 1 U transketolase). The reaction was initiated by adding D-ribulose-5-phosphate 3-epimerase (0.5 U) and incubated at 25°C for 30 minutes. The absorbance was read at 340 nm using a multi-detection microplate reader.

ADP-binding assay

Purified PRPS1 or PRPS2 proteins were incubated with 4 μCi of [^{14}C]ADP for 12 h at 4 °C in 100 μl binding buffer (50 mM Tris-HCl, pH 7.5, 100 mM KCl, 50 mM $MgCl_2$, 1 mM Na_3VO_4, 1 mM DTT, 5% glycerol) with shaking. The proteins were then washed twice with 0.5 ml of ice-cold binding buffer, and PRPS1 or PRPS2-associated radioactivity was detected through liquid scintillation counting.

Analyses of NHEJ and HR repair efficiency

NHEJ and HR repair was analyzed following previous reports (Jiang et al., 2015) and a schematic of this assay is presented in Figure S6A. Briefly, DR-GFP was introduced into HOK cells, WT and mutated FHs 74 Int cells as described elsewhere (Pierce et al., 1999). DR-GFP was prevented from being expressed due to the existence of the I-SceI site. Expression of I-SceI induces a DSB in the DR-GFP locus. PCR products were amplified using primers targeting the flanking sequences of the I-SceI site, and were then subjected to I-SceI and BcgI double enzyme digestion. NHEJ repair destroyed the I-SceI site and enabled the PCR product to be resistant to both I-SceI and BcgI digestion, resulting in a 0.65-kb PCR band. HR repair replaced the I-SceI-damaged sequence with a BcgI site, which restored GFP expression.

DR-GFP-expressing cells were transiently transfected with a vector expressing I-SceI. 36 h after transfection, the cells were treated with NU7441 (1 μM) and KU55933 (10 μM) for 12 h, which inhibited DNA repair and allowed accumulation of I-SceI-mediated DSBs, and were then subjected to ionizing radiation. For measurement of NHEJ repair, cells were incubated with lovastatin for 24 h before irradiation. Equal amounts of PCR products were subjected to I-SceI and BcgI digestion, and the ratio between the amounts of 0.65-kb and 0.5-kb digestion products were compared. For measurement of HR repair, cells were stained with Hoechst 72 h after irradiation and the percentage of GFP-positive cells was calculated as GFP-positive cells/Hoechst-positive nucleus. For measurement of I-SceI cleavage efficiency, the genomic DNA was extracted immediately after irradiation. The amount of 0.65-kb PCR products, which resulted from the naïve I-SceI-uncut DNA, gave an indirect value of I-SceI-induced DSBs (top part in Figure S6A). β-actin was used as an internal control. The sequences of primers were as follows: DR-GFP-F, 5-CTG CTA ACC ATG TTC ATG CC-3; DR-GFP-R, 5-AAG TCG TGC TGC TTC ATG TG-3; β-actin-F, 5-CAT GTT TGA GAC CTT CAA CAC CC; β-actin-R, AGG AAG GAA GGC TGG AAG AGT G. PCR bands were quantified using Image J software.

Analyses of NER repair efficiency

NER repair efficiency was measured following a previous report (Shen et al., 2014). Briefly, a CPD-containing DNA duplex was transfected into cells, and then retrieved. The repaired and unrepaired DNA duplex were quantified by qPCR with distinct primers, since Taq polymerase activity in qPCR amplification could be blocked by the CPD adduct (Wellinger and Thoma, 1996) (Figure S6J).

The oligos used to construct the CPD-containing DNA duplex were synthesized according to the following sequences (Figure S6J): oligo 1, 5-biotin-GCA CGT CAG GCA CGG CGT CGG TAC CAG CTG CGG CAA GGC CGG ATC CAG AC-3; 30-nt CPD-containing oligo 2, 5-P-CTC GTC AGC ATC TTC ATC ATA CAG TCA GTG-3, where CPD is underlined; oligo 3, 5-P-GTC CGC TCG AGA CAC CGA AAA CGG TGT CTC GAG CGG ACC ACT GAC TGT ATG ATG AAG ATG CTG ACG AGG TCT GGA TCC GGC CTT GCC GCA GCT GGT AC-ddC-3. The three oligos were hybridized together at equivalent molarities by boiling and re-annealing in a water bath. T4 DNA ligase was used to seal the nicks between the oligomers and complete the hairpin-like DNA duplex. A CPD-free oligo with the

same sequence of oligo 2 was synthesized to produce a naive DNA duplex with oligo 1 and 3, which was used in Figure S6K as a positive control.

After UVC treatment, the DNA duplex was immediately transfected into cells, and the cells were cultured in dark for 6 h. Nuclei were then isolated by using Nuclear/Cytosol Fractionation Kit (BioVision), and the DNA duplex was extracted by DNA extraction kit (Stratagene). The DNA duplex was further purified by streptavidin beads (Invitrogen), and then eluted by incubation at 80 °C in deionized water.

Real-time quantitative PCR (qPCR) reactions was performed to measure NER efficiency. DNA Engine Opticon 2 (MJ Research) was used to carry out real-time quantitative PCR (qPCR) reactions. DNA and primers were mixed with Brilliant III Ultra-Fast SYBR Green qPCR Master Mix (Agilent) following the manufacturer's instructions and PCR cycling was typically run with the following protocol: hot-start, 95°C, 3 min; cycling, 95°C, 5 sec and 60°C, 15 sec, 50 cycles; completion, 72°C, 1 min; melting curve, 60°C to 95°C, recording 0.2°C/sec. Primers were synthesized according to the following sequences: primer a, 5-GCA CGT CAG GCA CGG CGT C-3; primer b, 5-TTC GGT GTC TCG AGC GGA C-3; primer c, 5-GTC TGG ATC CGG CCT TGC C-3.

Since the CPD adduct blocks Taq polymerase activity in qPCR amplification (Wellinger and Thoma, 1996), only the repaired DNA duplex could be amplified and quantified with primer a/c. In contrast, both repaired and unrepaired DNA duplex could be amplified and quantified with primer a/b. Thus, the repair efficiency, which is defined as % repaired, can be calculated from the ratio of the level of the repaired DNA duplex to the level of total DNA duplex retrieved. The freshly prepared CPD-containing DNA duplex and the CPD-free (naive) DNA duplex were used in the qPCR amplification as negative and positive control, respectively.

Analyses of cellular gap-filling DNA synthesis

We used a two-step method to measure the gap-filling efficiency in WT or PRPS1/2-mutated cells following previous reports (Krishna et al., 2005; Mosbaugh and Linn, 1984) with some modifications. Briefly, DNA duplex containing a 4-nt single-strand gap were transfected into cells, retrieved, and then applied to an *in vitro* gap filling assay using radioactive dNTPs. Since radioactive dNTPs could only be incorporated into unfilled or partially filled DNA duplex, the normalized radioactivity of the DNA duplex indirectly indicates the efficiency of gap filling in cells (Figure S6L).

The oligos used to construct the DNA duplex with a 4-nt gap were synthesized according to the following sequences (Figure S6L): oligo 1, 5-biotin-GCA CGT CAG GCA CGG CGT CGG TAC CAG CTG CGG CAA GGC CGG ATC CAG ACC TCG TCA GCA TCT TCA TCA TAC AGT-3; oligo 2, 5- GGT CCG CTC GAG ACA CCG AAA ACG GTG TCT CGA GCG GAC CAC TGA CTG TAT GAT GAA GAT GCT GAC GAG GTC TGG ATC CGG CCT TGC CGC AGC TGG TAC-ddC-3, where the reverse complementary sequence of the 4-nt single-strand gap was underscored. The two oligos were hybridized together at equivalent molarities by boiling and re-annealing in a water bath. An oligo with the sequence 5-biotin-GCA CGT CAG GCA CGG CGT CGG TAC CAG CTG CGG CAA GGC CGG ATC CAG ACC TCG TCA GCA TCT TCA TCA TAC AGT CAG TGG TCC GCT CGA GAC ACC GAA AAC GGT GTC TCG AGC GGA CCA CTG ACT GTA TGA TGA AGA TGC TGA CGA GGT CTG GAT CCG GCC TTG CCG CAG CTG GTA C-ddC-3 was synthesized to produce a DNA duplex without gap.

After IR treatment, the DNA duplex was immediately transfected into cells. 1 h after transfection, nuclei were isolated by using a Nuclear/Cytosol Fractionation Kit (BioVision), and the DNA duplex was extracted by a DNA extraction kit (Stratagene). The DNA duplex was further purified by streptavidin beads (Invitrogen), and then eluted by incubation at 80 °C in deionized water.

The retrieved DNA duplex was then applied to an *in vitro* gap filling assay by incubation with 20 mM HEPES pH 7.5, 1 mM $MgCl_2$, 0.1 mM DTT, 0.1 mg/mL bovine serum albumin, 2% glycerol, 0.1 mM dATP, 0.1 mM dCTP, 0.1 mM dGTP, 0.1 mM dTTP, [α-^{32}P]dATP (750 Ci/mmol), [α-^{32}P]dCTP (750 Ci/mmol), [α-^{32}P]dGTP (750 Ci/mmol), [α-^{32}P]dTTP (750 Ci/mmol), and excessive rat liver recombinant pol β at 30°C for 1 h. The DNA duplex was further purified by excessive streptavidin beads (Invitrogen), and the radioactivity was detected through liquid scintillation counting. The freshly prepared DNA duplex with a 4-nt gap (Gap-DNA duplex), which have the maximum incorporation of radioactive dNTPs, was used in this *in vitro* gap-filling assay as negative control to mimic the DNA duplex that were completely unfilled in cells. The freshly prepared DNA duplex without the 4-nt gap (naive DNA duplex), which have no incorporation of radioactive dNTPs, was used as positive control to mimic the DNA duplex that were completely filled in cells.

The amount of DNA duplex was quantified by qPCR with primer a/b. Primers are synthesized according the following sequences: primer a, 5-GCA CGT CAG GCA CGG CGT C-3; primer b, 5-TTC GGT GTC TCG AGC GGA C-3. The radioactivity was normalized to the amount of DNA duplex. Since the radioactive dNTPs can only be incorporated during the *in vitro* gap filling assay, the gap filling efficiency in cells was calculated by the following formula:

$$\text{Gap filled in cell}\ (\%) = \frac{\text{normalized radioactivity}\ (\text{freshly prepared gap DNA}) - \text{normalized radioactivity}\ (\text{retrieved DNA})}{\text{normalized radioactivity}\ (\text{freshly prepared gap DNA})}$$

Liposome-encapsulated deoxyribonucleotide delivery

Encapsulation of deoxyribonucleotides into liposomes was carried out according to a published protocol (Zhou et al., 2012). In brief, a chloroform solution of phosphatidylcholine (0.26 mM), cholesterol (0.12 mM), and 1,2 dioleoyl-3-trimethyl-ammonium-propane (10.8 mM) was evaporated, and the film formed was hydrated with 5 mL of 600 mM dATP, dCTP, dTTP, or dGTP in Krebs-Henseleit (KH) buffer. The dispersion was frozen at –80°C for 30 minutes followed by thawing at 45°C for 5 minutes, and this cycle was repeated 5 times. Each deoxyribonucleotide-loaded liposome was separated by dialysis against KH buffer at 48°C overnight. After indicated irradiation, four deoxyribonucleotide-loaded liposomes were added into cell culture. The cells were incubated for 10 min. The

amounts of each deoxyribonucleotide-loaded liposome were optimized by pilot testing to induce a desired cellular level in different experiments.

Clonogenic survival assay

24 h after the indicated treatment, clonogenic survival assays were performed by seeding 100 cells in one well of a six-well plate. After culture for 14 days, cells were fixed and stained with crystal violet solution (0.5% crystal violet in 20% ethanol). Clones containing more than 50 cells were counted.

CCK8 assay

Cell proliferation was measured by a Cell Counting Kit 8 (WST-8/CCK-8) (Abcam). Briefly, 5000 cells were seeded in one well of a 96-well plate, and incubated overnight. On day 0, the cells were treated with ionizing radiation, and then cultured for 3 days. To measure cell proliferation, 10 μl WST-8 solution was added to one well at day 0 (before irradiation) or at the indicated time points. The 96-well plate was then incubated for 3 hours at 37°C in the dark. The absorbance was then measured at 460 nm, and normalized to the value at day 0.

Cell survival assays

16 h after irradiation, a cell suspension of neutrophil cells was mixed with 0.2% trypan blue solution at 1:1, and incubated at room temperature for 3 min. A drop of the trypan blue/cell mixture was applied to a hemocytometer. The numbers of unstained and stained cells were counted. The survival ratio was calculated as the unstained cell number/(unstained cell number + stained cell number).

Animal study

Male C57BL/6 mice, aged 6-8 weeks and weighing 18-22 g, were used for whole body or abdominal irradiation with a Cr^{137} γ-ray irradiator (Atomic Energy of Canada, Chalk River, Ontario, Canada). Mice were exposed to 12 or 4.5 Gy ionizing radiation at 2 Gy/min at room temperature. To examine phosphorylation of PRPS1/2, mice were sacrificed 4 h after irradiation. The intestine and salivary gland tissues were obtained, fixed and used for IHC staining with the indicated antibodies. Neutrophil cells were isolated from bone marrow tissues by using a Neutrophil Isolation Kit (Miltenyi Biotec) and used for immunoblots. To examine cell viability, mice were sacrificed 72 h after irradiation. The intestine and salivary gland tissues were obtained, fixed and used for Ki67 IHC staining. The cell survival rate for bone marrow-derived neutrophil cells was measured by trypan blue staining. For the metabolic flux assay, mice were fasted overnight, intraperitoneally injected with 0.3 M [$^{13}C_6$]-glucose (200 μl/20 g), and then immediately subjected to irradiation. The intestine tissue, salivary gland tissue or bone marrow-derived neutrophils were collected 3 h after irradiation. The *STING* knockout mice were obtained from GemPharmatech (Nanjing, China). The animals were treated in accordance with relevant institutional and national guidelines and regulations. The use of animals was approved by the institutional review board of Chengdu Medical College.

Diarrhea assessment

Mice were assessed 5 days after abdominal irradiation according to previous grades (Gibson et al., 2005). Briefly, there were 4 scores: 0, no diarrhea; 1, mild diarrhea (staining of anus); 2, moderate diarrhea (staining over the top of the legs and lower abdomen); and 3, severe diarrhea (staining over the legs and higher abdomen, often associated with continual oozing).

Immunohistochemical staining

The immunohistochemical staining was performed using the VECTASTAIN ABC kit (VECTOR LABORATORIES, CA) according to the manufacturer's instructions. We quantitatively scored the tissue sections according to the percentage of positive cells and staining intensity, as previously defined (Lee et al., 2018). We assigned the following proportion scores: 0 if 0% of the tumor cells showed positive staining, 1 if 0% to 10%, 2 if 11% to 30%, 3 if 31% to 70%, and 4 if 71% to 100%. We also rated the intensity of staining on a scale of 0 to 4: 0, negative; 1, weak; 2, moderate; 3, strong; and 4, very strong. We then multiplied the proportion and intensity scores to obtain a total score (range: 0-16).

QUANTIFICATION AND STATISTICAL ANALYSIS

All quantitative data are presented as the mean and SD. A 2-group comparison was conducted using a 2-sided, 2-sample Student t test. Comparisons that were statistically significant were labeled with * ($P < 0.05$), ** ($P < 0.01$), or *** ($P < 0.001$). Statistical analyses were performed by using GraphPad Prism (Version 9).